

**ACOUSTIC VIBRATION FIBER SENSOR FOR PIPELINE LEAKAGE
DETECTION**

ONG KANG SHEN

**A project report submitted in partial fulfilment of the
requirements for the award of Bachelor of Engineering
(Hons.) Electrical and Electronic Engineering**

**Lee Kong Chian Faculty of Engineering and Science
Universiti Tunku Abdul Rahman**

January 2017

DECLARATION

I hereby declare that this project report is based on my original work except for citations and quotations which have been duly acknowledged. I also declare that it has not been previously and concurrently submitted for any other degree or award at UTAR or other institutions.

Signature : _____

Name : ONG KANG SHEN

ID No. : 1308145

Date : 19 / 9 / 2017

APPROVAL FOR SUBMISSION

I certify that this project report entitled “**ACOUSTIC VIBRATION FIBER SENSOR FOR PIPELINE LEAKAGE DETECTION**” was prepared by **ONG KANG SHEN** has met the required standard for submission in partial fulfilment of the requirements for the award of Bachelor of Engineering (Hons.) Electrical and Electronic at Universiti Tunku Abdul Rahman.

Approved by,

Signature : _____

Supervisor : Mr. Lin Horng Sheng

Date : 19 / 9 / 2017

The copyright of this report belongs to the author under the terms of the copyright Act 1987 as qualified by Intellectual Property Policy of Universiti Tunku Abdul Rahman. Due acknowledgement shall always be made of the use of any material contained in, or derived from, this report.

© 2017, Ong Kang Shen. All right reserved.

ACKNOWLEDGEMENTS

I would like to thank everyone who had contributed to the successful completion of this project. I would like to express my gratitude to my research supervisor, Mr. Lin Horng Sheng for his invaluable advice, guidance and his enormous patience throughout the development of the research.

Furthermore, I am grateful to the members of Photonics Research Group, UTAR for their help and support throughout the research. They are Assoc. Prof. Dr. Pua Chang Hong, Mr. Png Wen Hao and Mr. Law Zi Jian.

In addition, I would also like to express my gratitude to my loving parents and friends who had helped and given me encouragement in completing this final year project.

ABSTRACT

Any minor defects in the pipeline system might cause severe impacts on financial, nature environment and casualties. Consequently, leakage detection plays important role in the context of environmental, personnel safety and pipeline security. The limitations of current detection technologies are usually higher in cost, low sensitivity in detection of small scale deformation and difficulty in implementation. Over the years, fiber optic has drawn much attention due to its unique congenital advantages having not only high adaptability in environments of electromagnetic interference, chemical corrosion and high temperature but also light in weight, compact in size and applicable for distributed measurement in long distance. In this project, an incredibly simple configuration and effective acoustic vibration sensor based on macro-bend coated fiber (SMF-28) for pipeline leakage detection is proposed and developed. The proposed fiber sensor is configured by just bending the fiber to form a small loop in free space. It fully utilizes the undesirable loss e.g. bend loss as sensing mechanism by allowing the perturbation (acoustic vibration) to induce optical power losses through the bend fibers. The optical power loss is varied accordingly to the shift of location of the coupling between the core and leaky mode. Various measurements have been carried out to obtain the optimum bend radius (5.0 mm) for the fiber sensor and in the following vibration test it shows promising results which are capable to detect vibrations at the frequency range of 20 Hz to 2500 Hz. In the field test, the bend coated fiber sensor shows effective detection in leakage at low pressure water pipe with the leak size of a few millimeters.

TABLE OF CONTENTS

DECLARATION	ii
APPROVAL FOR SUBMISSION	iii
ACKNOWLEDGEMENTS	v
ABSTRACT	vi
TABLE OF CONTENTS	vii
LIST OF TABLES	x
LIST OF FIGURES	xi
LIST OF SYMBOLS / ABBREVIATIONS	xiv
LIST OF APPENDICES	xv

CHAPTER

1	INTRODUCTION	1
	1.1 Background	1
	1.1.1 Pipeline Leakage Detection	1
	1.1.2 Fiber Optic Sensor (FOS) in SHM	3
	1.1.3 Installation of FOS in SHM	3
	1.1.4 Basic Concept of FOS System	3
	1.2 Problem Statement	4
	1.3 Aims and Objectives	5
	1.4 Scope and Limitation of the Study	5
	1.5 Contribution of the Study	6
	1.6 Outline of the Report	6
2	LITERATURE REVIEW	7
	2.1 Introduction	7
	2.2 Fundamentals in Waveguiding	7
	2.3 Types of FOS in SHM Acoustic Detection	9

2.3.1	Single Taper Fiber Acoustic Vibration Sensor	11
2.3.2	Single – Multi – Single mode (SMS) Fiber Sensor	12
2.3.3	Fiber Bragg Grating (FBG) Sensors for Acoustic Emission in SHM	14
2.3.4	Intensity-Modulated Based Bend Fiber Optic Sensor	15
2.4	Comparison of FOSs	19
2.5	Design of Bend Coated Fiber Sensor	20
2.5.1	Fabrication Criteria	20
3	METHODOLOGY AND WORK PLAN	21
3.1	Introduction	21
3.2	Flow Chart of the Work Plan	22
3.3	Design and Fabrication of Sensor	22
3.3.1	Design of Sensor	23
3.3.2	Fabrication of Sensor	23
3.4	Characterisation of Sensor	24
3.4.1	Measurement of Losses on Various Bend Radius	24
3.4.2	Measurement of Losses on Various Wrapping Turns	25
3.5	Implementation of Sensor in Acoustic Vibration Test	26
3.6	Implementation of Sensor in Field Test (Water Pipeline)	27
4	RESULTS AND DISCUSSIONS	28
4.1	Bending Loss Measurements	28
4.1.1	Bend Radius Dependent Property of the Sensor	28
4.1.2	Number of Wrapping Turns Dependent Property of the Sensor	30
4.2	Acoustic Vibration Test	32
4.2.1	Background Signal	33
4.2.2	Acoustic Vibration Signals	34
4.3	Field Test (Water Pipeline)	40
4.4	Summary	48

5	CONCLUSIONS AND RECOMMENDATIONS	49
5.1	Conclusions	49
5.2	Recommendations for Future Work	49
	REFERENCES	51
	APPENDICES	54

LIST OF TABLES

TABLE	TITLE	PAGE
1.1	2017 Worldwide pipeline constructions (Tubb, 2017)	1
2.1	Evaluation of types of FOS	19
2.2	Optimum parameters for the bend loss sensor (Shahami, Siti Azlida and Dambul, 2016)	20
4.1	Parameters of Corning SMF-28 fiber at wavelength 1550 nm	29
4.2	The increment of intervals for the frequency range	34

LIST OF FIGURES

FIGURE	TITLE	PAGE
1.1	Pipeline incidents over 20 years trend (PHMSA, 2011)	2
1.2	Schematic diagram of the FOS system (Righini, Tajani and Cutolo, 2009)	4
2.1	Planar dielectric slab waveguide with central region of refractive index, n_1 sandwiched between 2 semi-infinite regions of refractive index, n_2 (Kasap, 2001)	7
2.2	Propagated light wave in the planar dielectric guide (Kasap, 2001)	8
2.3	The responses of fiber taper sensor to acoustic wave at 1 kHz in (a) time and (b) frequency spectrum (Xu et al., 2012)	12
2.4	Overall structure of the SMS fiber sensor (Xu et al., 2011)	13
2.5	The FFT spectrum at (a) 30.039 kHz and (b) 35.156 kHz (Xu et al., 2011)	14
2.6	Wavelength-selective reflectional filter of FBG (Rajan, 2015)	15
2.7	The change in light intensity for bend fiber (Gambling and Matsumura, 1978)	16
2.8	Relative output power against displacement for FOLS (6, 7 and 8 mm loop) and the zoom in view for the linear region within one intermediate peak of 8 mm FOLS (Nishino, Chen and Gupta, 2014)	17
2.9	Experimental setup of FOLS calibration arrangement (Nishino, Chen and Gupta, 2014)	18
2.10	Frequency response of FOLS at 10 and 100 Hz (Nishino, Chen and Gupta, 2014)	19
3.1	Flow chart for overall project of acoustic vibration fiber sensor for pipeline leakage detection	21

3.2	The work plan for the development of bend coated fiber sensor	22
3.3	Configuration of the bend-coated fiber sensor	23
3.4	The Sumitomo fusion splicer and cleaver	23
3.5	Bending loss measurement setup	24
3.6	The reference value of the optical power meter is set to 0.00 dB	25
3.7	Losses display on the power meter due to the bending of fiber	25
3.8	The setup for measuring bend loss at different number of wrapping turns on a mandrel	26
3.9	Experimental setup for acoustic vibration test	27
3.10	Experimental setup for the field test	27
4.1	Relationship between the bend loss and correspond bend radius at 1550 nm wavelength	29
4.2	The relationship of power loss against wrapping turns, N for bend radius, R equals to 8, 10, and 12 mm	31
4.3	The inter-relationship between the bend radius and wrapping turns against the bending loss	32
4.4	The bend coated fiber sensor with bending radius of 2.5, 5.0 and 7.5 mm	33
4.5	The background signal of the fiber sensor from 0 to 1000 Hz	34
4.6	Frequency response of 2.5 mm sensor at frequency range of (a) 20 Hz to 100 Hz & (b) 200 Hz to 600 Hz	35
4.7	Frequency response of 5.0 mm sensor at frequency range of (a) 20 Hz to 100 Hz (b) 200 Hz to 1000 Hz (c) 1000 Hz to 1800 Hz & (d) 2000 Hz to 2600 Hz	38
4.8	Frequency response of 7.5 mm sensor at frequency range of (a) 20 Hz to 100 Hz (b) 200 Hz to 1000 Hz & (c) 1000 Hz to 1600 Hz	39

4.9	Background signals for field test	41
4.10	(a) No leak & (b) leak signals for 2.5 mm radius fiber sensor	43
4.11	(a) No leak & (b) leak signals for 5.0 mm radius fiber sensor	45
4.12	(a) No leak & (b) leak signals for 7.5 mm radius fiber sensor	47
4.13	Leak signals of the fiber sensor at radius of 2.5, 5.0 and 7.5 mm	48

LIST OF SYMBOLS / ABBREVIATIONS

BOK	body of knowledge
FOLS	fiber optic loop sensor
FOS	fiber optic sensor
MFL	magnetic flux leakage
NA	numerical aperture
PZT	piezoelectric transducer
SHM	structural health monitoring
SMF	single-mode fiber
SMS	single – multi – single mode
SNR	signal-to-noise ratio
TIR	total internal reflection

LIST OF APPENDICES

APPENDIX A: CALCULATION OF MINIMUM CRITICAL BEND RADIUS FOR SINGLE MODE FIBER	54
APPENDIX B: CORNING SMF-28 DATA SHEET	55

CHAPTER 1

INTRODUCTION

1.1 Background

1.1.1 Pipeline Leakage Detection

As one of the most commonly used transportation method, pipeline constructions continue to growth over the years. By year 2017, it is indicate that 134,866 km of pipeline projects are planned and under construction worldwide. Among these, 61,783 km of pipeline projects are still under planning and design phase, while, the rest 73,084 km are in various stages of construction as illustrated in Table 1.1 (Tubb, 2017).

Table 1.1: 2017 Worldwide pipeline constructions (Tubb, 2017)

	Pipeline under construction (km)	New and planned pipeline (km)
North America	24,589	26,611
Central America & Caribbean	2,931	4,601
Africa	2,762	3,650
Asia Pacific	16,230	15,696
Post-Soviet States & Eastern Europe	17,220	3,228
Middle Eastern	7,118	7,715
European Union	2,234	282
Total	73,084	61,783

However, along with the development and wide application of pipelines, the pipeline network system security has become a vital issue. Various incidents such as water pipe dehiscence, gas pipe explosion and oil pipe leakage have been reported from 1997 to 2016 as shown in Figure 1.2 (PHMSA, 2011). Any minor defects in the pipeline system might cause severe impact on the country's economy, nature environment and casualties (Wang, Lambert, Simpson and Vitkovsky, 2001). Hence, with the aids of Structural Health Monitoring (SHM), inspection or repairing works can be carried out at pre-defined stage in order to safeguard the structural integrity of the pipeline system.

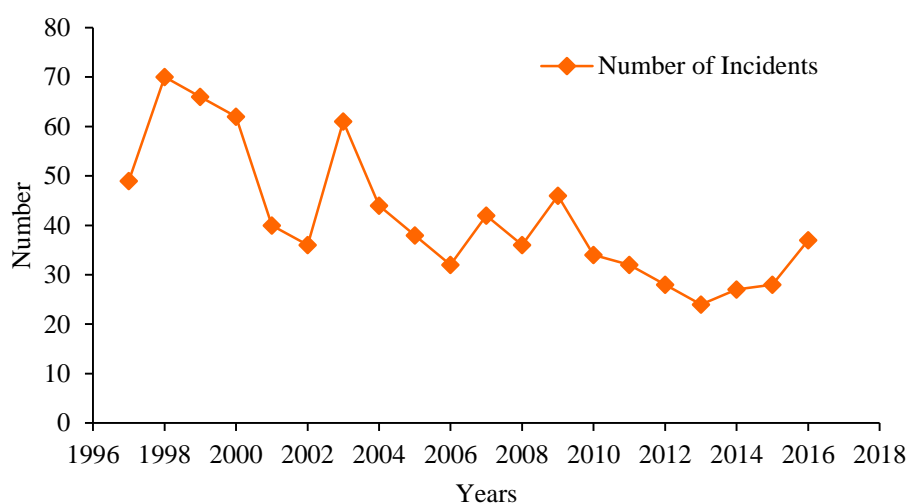


Figure 1.1: Pipeline incidents over 20 years trend (PHMSA, 2011)

SHM is a process of acquisition of information and implementing a damage detection strategy in engineering infrastructure in order to allow the processes of diagnosis and prognosis of structural integrity. Besides, SHM also defined as the monitoring of the integrity of a structure in order to mitigate the hazard due to various factors such as live load, ocean, waves, earthquake, fatigue, heat, ageing and others (Chung, 2001).

Through SHM, the stability and solidity of an infrastructure during its service life are evaluated to ensure the infrastructure serviceability and sustainability. The dynamic response of the infrastructure is recorded directly and hence the infrastructure condition or performance can be identified.

For pipeline leakage detection, different detection technologies are implemented such as magnetic flux leakage (MFL) detection, piezoelectric transducers (PZTs) and current sensor. These sensors will generate waves propagate through the structure and reflected back when meeting cut-offs such as structural flaws. By analysing the reflected wave's information, the structure health condition can be identified. Nevertheless, due to the damping of materials or structural causes attenuation in the waves during propagation. This will weaken the signal and incur error in exhibit damage index even if the damage is severe (Yang, Hu and Lu, 2008).

1.1.2 Fiber Optic Sensor (FOS) in SHM

Over the past several decades, FOSs have drawn much attention due to its unique congenital advantages. The fiber optic sensor not only having high adaptability in environments of electromagnetic interference, chemical corrosion and high temperature but also can deploy for distributed measurement in long distance (Lee, 2003). Furthermore, high sensitivity of fiber optic sensor in detecting a small scale deformation predominate other types of sensing methods.

1.1.3 Installation of FOS in SHM

Generally, sensing system of fiber optic sensor in SHM can be divided into localized and distributed sensing. In localized sensing system, only a pre-determined point is detected and the measured signal is feedback to the system. While, for distributed sensing system large number of localized fiber optic sensors which formed a sensing array is used to detect multiple points. This greatly enhance the magnitude of the measurand. However, multiplexing techniques are required in distributed sensing system to discriminate the output data from the sensing array (Yin and Yu, 2002).

1.1.4 Basic Concept of FOS System

Perturbations from the external environment will cause modulation to the light wave that propagates along the waveguide even though the light waves are said to be ‘confined’ within the optical fiber. Much useful information draws from the perturbations for sensing purposes. As a matter of fact, the interaction between the measurand and the optical fiber creates a modulation to the light waves that propagate along the waveguide. This modulation denotes the function of the measurand of interest (Righini, Tajani and Cutolo, 2009).

Figure 1.2 depicts the structures of the fiber optic sensor system in application. The basic elements comprise of: a laser source, the waveguides (i.e. fiber optic) in which the perturbations induced modulation of the light waves, photo-detector and signal processing unit.

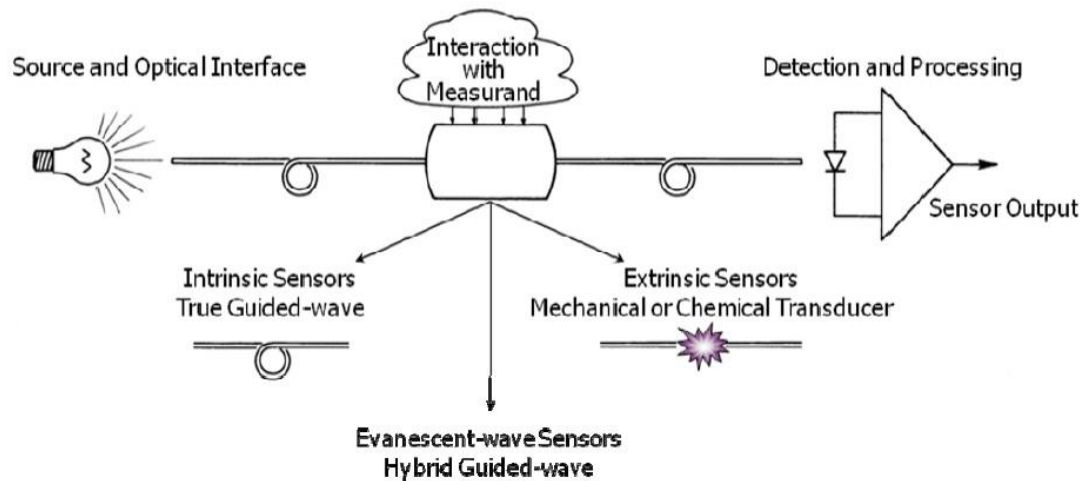


Figure 1.2: Schematic diagram of the FOS system (Righini, Tajani and Cutolo, 2009)

1.2 Problem Statement

As the public scrutiny on pipeline system integrity increases, the safety of operating pipelines has become one of the most important issues in the field of industrial. Leakage in pipeline system can cause tremendous loss and even environmental damage if the leakage is unable to be detected immediately. However, the conventional pipeline detection technologies such as MLF and current sensor depends on the transmission medium (inline inspection) as driving force (Yang, Liu, Zhang and Gao, 2009). The pipeline operation needs to be shut down and the restriction inside the pipeline would have to be cleared before starting the inspection (Reed, Robinson and Smart, 2004).

Furthermore, pipeline monitoring usually limited to visual inspection, hence it is hard to detect and locate small scale pipeline failures. Consequently, the failures are being detected only when there are severe damages on the pipeline or the output flow is affected due to failures (Wang et al., 2001).

1.3 Aims and Objectives

The aim of this research is to design and develop an effective surface mounted fiber sensor that is able to detect low frequency acoustic vibration signal induced due to pipeline leakage or deformation. The objectives of this project are:

- (i) To investigate the bending loss as sensing mechanism of the fiber sensor based on single-mode fiber (SMF).
- (ii) To characterize the fiber sensor with different measurements.
- (iii) To detect and recognized the acoustic wave pattern of background, no leak and leak signals by implementing the fiber sensor in field test (water pipeline).

1.4 Scope and Limitation of the Study

It is too wide for a study or research under a limited time frame to cover all the subjects that are broadly related. As well known, research is a lifelong learning and continuing effort, hence, the present work focused on the determined scope as aforementioned.

The literature review mainly focuses on the behaviour of propagating light in the optical fiber, various sensing mechanisms of fiber sensor on vibration measurement and finding out the related technologies and tools. Throughout the study, the related theory and technology were reviewed and compared.

Before developing the fiber sensor, different measurement system for the characterization of fiber sensor has been planned and examined. At the developing stage, the fiber sensor is characterized using the determined measurement systems to obtain optimum performance in acoustic vibration sensing. Finally, the fiber sensor was implemented in field test and the result is observed and analysed.

Although the research has reached its aim, there were some unavoidable limitations. In this research, the field test was conducted only on the water pipeline. Therefore, to generalize the results, the study should involve other types of pipeline. Besides, a proper packaging for the bend coated fiber sensor was necessary to segregate unwanted perturbation from the environment exert on the sensor. At last but not least, an automation system for the leak signal processing is needed to cut down the interval for repetitive operation of whole system.

1.5 Contribution of the Study

The purpose of this research is to contribute to the body of knowledge (BOK) on current technologies in pipeline leakage detection by proposing a simple yet effective vibration sensor based on optical fiber.

This research intended to shift the focus on other configurations of fiber sensors to macro-bending in optical fiber and this has led to the development of fiber sensor which employs macro-bend where it is simple configured and effective in vibration sensing. This ring configured fiber sensor is able to detect the vibration frequency from 20 Hz to 2500 Hz. Furthermore, through the characterization, the bending radius of the fiber at 5 mm is the optimum design for the sensor. To my best of knowledge, this is the first time implementation of the bend coated fiber sensor on field test.

1.6 Outline of the Report

In Chapter 1, brief introduction on background of pipeline detection methods, SHM, types and sensing principals of FOS is described and outlines the problem statement, objectives and layout of the report.

Chapter 2 discusses the literature review of types of FOS in SHM acoustic detection and comparison of these sensors on different criterion. For Chapter 3, the methodology on the fabrication and configuration of the bend coated fiber sensor and the characterization of sensor is discussed in details.

Chapter 4 investigates the power intensity changes in corresponding to the curvature radius and number of turns of fiber wrap on a mandrel. Besides, the fiber sensor is implemented in acoustic vibration test and field test to obtain its sensing range and pattern of the transmitted acoustic waves. The results of respective measurements are further analysed and discussed in this section as well.

Chapter 5 summarizes the works that have been done in whole project and provide some directions for future improvement.

CHAPTER 2

LITERATURE REVIEW

2.1 Introduction

In this chapter, a brief description of the fundamentals of waveguiding, types and operation of fiber optic (waveguide) sensor in SHM acoustic vibration detection will be elaborated. Single taper fiber, single-multi-single mode fiber, Fiber Bragg Grating (FBG) and intensity-modulated based bend fiber optic sensor is the sensor that dominantly researched. In the part hereof, the literature review based on the sensing principle (loss mechanism) and structural system of these types of sensor will be explained in detailed.

2.2 Fundamentals in Waveguiding

In order to understand the general property of the propagation of light wave in fiber optic the planar dielectric slab waveguide shown in Figure 2.1 is considered. The planar dielectric with thickness of $2a$ has a central rectangular region of higher refractive index, n_1 which known as the core and surrounding region with lower refractive index, n_2 known as the cladding.

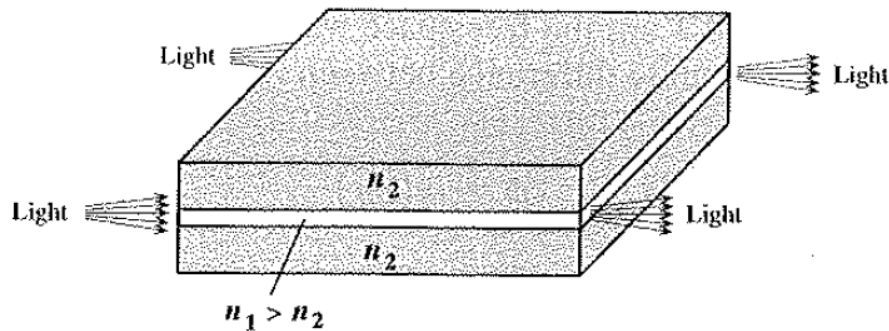


Figure 2.1: Planar dielectric slab waveguide with central region of refractive index, n_1 sandwiched between 2 semi-infinite regions of refractive index, n_2 (Kasap, 2001)

As the light propagate and passing through the planar waveguide, it experience total internal reflection (TIR) at the dielectric (n_1 and n_2) boundaries. TIR happens when the angle of incidence, θ_i of the light wave is greater than critical

angle θ_c . Considered a plane wave type of light ray, the light wave is guided in zigzag fashion as illustrated in Figure 2.2. On this light wave, constant phase wavefront is normal to the propagation direction. The specified light wave reflected at point B and C . The wavefront C overlaps the wavefront A on the original ray right after the reflection at point C . The two will interfere destructively and cancel off each other if both are in phase. Conversely, the constructive interference rises up only at certain reflection angle, θ .

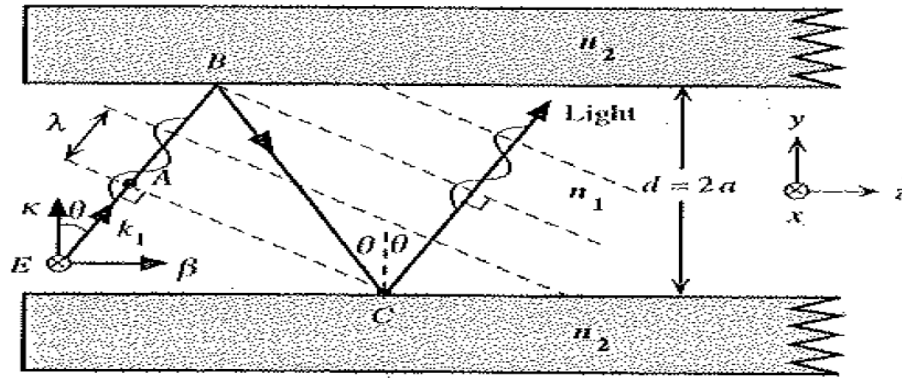


Figure 2.2: Propagated light wave in the planar dielectric guide (Kasap, 2001)

Basically, the phase difference between A and C must be a multiple of 2π for constructive interference and corresponds to the optical path length $AB+BC$ is given as below (Kasap, 2001):

$$\Delta\phi(AC) = k_1(AB + BC) - 2\phi = m(2\pi) \quad (2.1)$$

where k_1 , λ and m are the wave vector in medium n_1 ($k_1 = kn_1 = 2\pi n_1/\lambda$), free space wavelength and integer (0, 1, 2,...). From the geometric view, the optical path $AB+BC$ can be given as $2d \cos \theta$. Hence, equation (2.1) is rewrite into (Kasap, 2001):

$$k_1(2d \cos \theta) - 2\phi = m(2\pi) \quad (2.2)$$

Obviously, for equation (2.2), only specific values of θ and ϕ can satisfy for a given integer m and value of ϕ is dependent on θ . Thus, for each m , only one allowed angle θ_m and ϕ_m . The waveguide condition is obtained by dividing equation (2.2) by two.

$$\left[\frac{2\pi n_1(2a)}{\lambda} \right] \cos\theta_m - \phi_m = m\pi \quad (2.3)$$

Notwithstanding the waveguide condition in equation (2.3) identifies the permissible θ_m values, but the θ_m values must also fulfil the TIR condition, such that, $\sin \theta_m > \sin \theta_c$. In accordance with the second condition imposed, only a certain number of modes are being allowed in the waveguide. Based on equation (2.3), the expression for $\sin \theta_m$ is obtained in addition of TIR condition ($\sin \theta_m > \sin \theta_c$) to reveal the allowable mode number, m (Kasap, 2001)

$$m \leq (2V - \phi)/\pi \quad (2.4)$$

where V also known as V -number and it is given by (Kasap, 2001):

$$V = \frac{2\pi a}{\lambda} (n_1^2 - n_2^2)^{\frac{1}{2}} \quad (2.5)$$

For the lowest mode where m equal to 0, the value of V is less than $\pi/2$, only the fundamental (or core) mode propagates along the dielectric slab waveguide. Such waveguide is also termed as the single-mode waveguide. The wavelength that leads to $V = \pi/2$ is known as the cut-off wavelength, λ_c .

2.3 Types of FOS in SHM Acoustic Detection

As mention earlier in the previous section, the light waves are transmitted and propagates through the optical fiber. However, the external environment will still be able to perturb the light waves that trapped inside the optical fiber. The interaction between the measurand (parameters of interest) with the optical fiber induced a variation to the optical waves that propagates in the waveguide. This modulation denotes a function of the interaction of measurand and fiber optic (Righini, Tajani

and Cutolo, 2009). Based on the modulation of the optical parameters that cause by the measurand, the FOS can be loosely grouped into few types:

(i) Phase modulation

Basically, the phase-modulated sensors are also known as interferometers whereby the interferometric schemes are used to measure the phase shift of the signal (Steele, 1983). The measurand that induced a phase shift, $\Delta\phi$ of the guided light wave with variation of optical fiber path length, ΔL can be expressed as follows with wavelength, λ (Righini, Tajani and Cutolo, 2009):

$$\Delta\phi = \frac{2\pi}{\lambda} \Delta L \quad (2.6)$$

(ii) Polarization modulation

The polarization-modulated sensors work based on the polarization mode-coupling due to the birefringence changes which act as perturbations on the optical fiber (Wolinski, 1999).

(iii) Wavelength modulation

Wavelength-modulated sensors depend upon the grating inscribed inside the optical fiber for detection. In other words, it uses the modulation in the wavelength of light in sensing the measurand (Fidanboylu and Efendioglu, 2009).

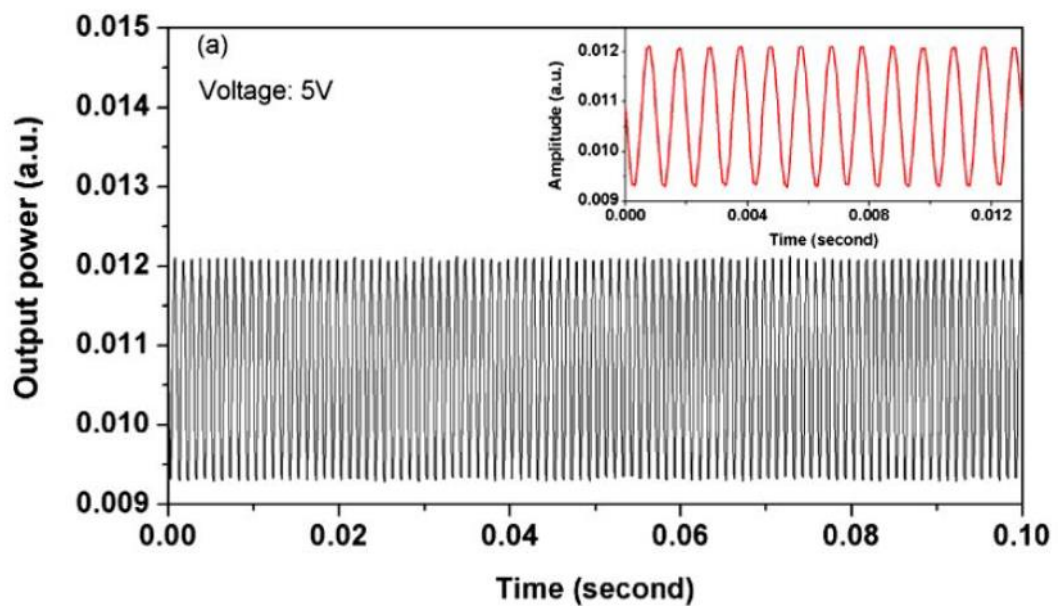
(iv) Intensity modulation

According to Polygerinos, the intensity of the light propagating through an optical fiber can be easily perturbed by reflectance, curvature, or different medium where the light is propagated. (Polygerinos, Seneviratne and Althoefer, 2011). As a result, the intensity-modulated sensors will utilize the loss mechanism in sensing the measurand. In addition, the FOSs can be subdivided into two kinds of sensors namely, extrinsic and intrinsic sensors. Extrinsic sensors consist of a transducer that coupled to the waveguide and modulates the light beam in response to the perturbation. For intrinsic sensors, it depends on the optical fiber itself as sensing element to the environmental effect (Yin and Yu, 2002).

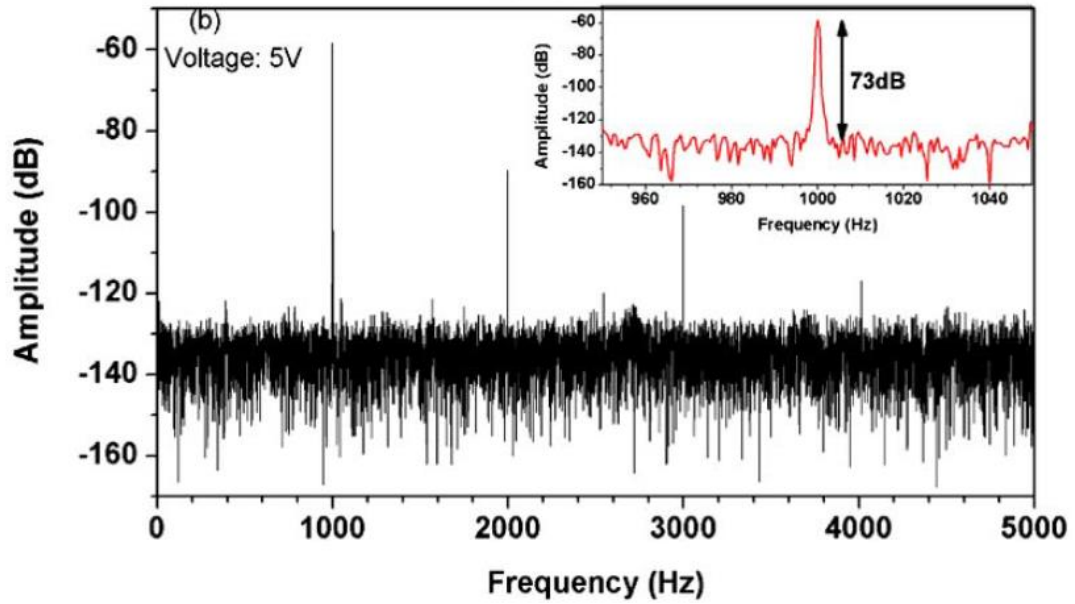
2.3.1 Single Taper Fiber Acoustic Vibration Sensor

A fiber optic vibration sensor with nonadiabatic tapered fiber is proposed and demonstrated by Xu, et al. The acoustic vibrations are able to be detected by measuring the output optical power of the taper. Besides, this single taper fiber sensor has a wide range of sensing frequency from Hz to kHz and the signal-to-noise ratio (SNR) is able to reach 73 dB. Figure 2.3 shows the results collected at both time and frequency domain of 1 kHz sinusoidal waveform acoustic source at 5 V. In the time domain, the output optical power varies uniformly as the sinusoidal waveform, thus, Fast Fourier Transform (FFT) is performed converting the time domain power to frequency domain. The demodulated frequency as illustrated in Figure 2.3 (b) shows that the harmonics are overcome by the tone of fundamental frequency. In other words, the induced vibration frequency is clearly shown in the frequency domain with significant SNR of 73 dB (Xu et al., 2012).

The abrupt biconical taper in this sensor acts as the multi-mode fiber and the fiber taper segment are exposed to acoustic waves. Therefore, displacement of the taper segment is induced by the acoustic vibrations. As a result, mode couplings occur not only in between the lower order modes (e.g. LP_{01} and LP_{02}) but in this case, the mode couplings also involve the high order modes as well (Snyder and Love, 1986).



(a)



(b)

Figure 2.3: The responses of fiber taper sensor to acoustic wave at 1 kHz in (a) time and (b) frequency spectrum (Xu et al., 2012)

2.3.2 Single – Multi – Single mode (SMS) Fiber Sensor

As reported by Xu et al., the SMS fiber sensor is used to sense the radiation of acoustic waves by implementing the multi-mode interference theory. Generally, the two lowest-order modes in optical fiber are used to achieve inter-modal interference as the complexity will increase for the interference more than two modes.

In SMF, owing to the circular symmetric feature in the core mode, the incoming source is assumed to have a field distribution of $E(r, 0)$ (Zhao, Jin and Liang, 2011). When the laser source is emitted into the multi-mode fiber core, the power of coherent laser will be decomposed into multiple eigenmodes, LP_{nm} in the fiber but these modes maintain at its relative phase coherence respectively. This is due to the additive and destructive interference of the mode of transmission. The mode fields are expressed as (Xu, Liang, Xu and Qu, 2011):

$$\Psi_{01} = A_{01}f_{01}(r)e^{(-i\beta_{01}+\beta_{01})} \quad (2.7)$$

$$\Psi_{11} = A_{11}f_{11}(r)\cos\varphi e^{(-i\beta_{11}+\beta_{11})} \quad (2.8)$$

where Ψ_{01} and Ψ_{11} is the field function for LP_{01} mode and LP_{11} mode respectively, A_{01} and A_{11} are the amplitude coefficients of the mode field, β_{01} and β_{11} are the propagation constant for LP_{01} and LP_{11} mode. Once the perturbation (i.e. acoustic emission) acts on the fiber, the modes of transmission in the fiber will be re-intervention and phase difference occurs between the modes causes the corresponding speckle intensity to change. The synthetic light intensity is:

$$I(r, \varphi) = A_{01}^2 f_{01}^2(r) + A_{11}^2 f_{11}^2(r) \cos^2 \varphi + 2A_{01}A_{11} \times f_{01}(r)f_{11}(r)\cos(\varphi)\cos(\Delta\beta\Delta L - \Delta\theta) \quad (2.9)$$

where ΔL is the length change by fiber axial tension, $\Delta\beta$ is the propagation constant difference ($\Delta\beta = \beta_{01} - \beta_{11}$) and $\Delta\theta$ is the two-mode phase difference. Figure 2.4 shows the overall structure of the SMS fiber sensor and the hit signal that produce from the PZT analog ultrasonic emitter is being detected by the sensor. Then, the results of the FFT spectrum at frequency of 30 kHz and 35 kHz are illustrated in Figure 2.5 whereby the measured frequency is equal to 30.029 kHz and 35.156 kHz.

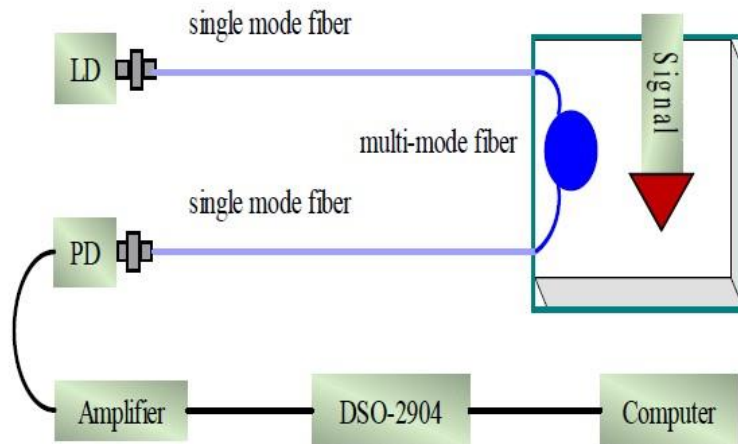


Figure 2.4: Overall structure of the SMS fiber sensor (Xu et al., 2011)

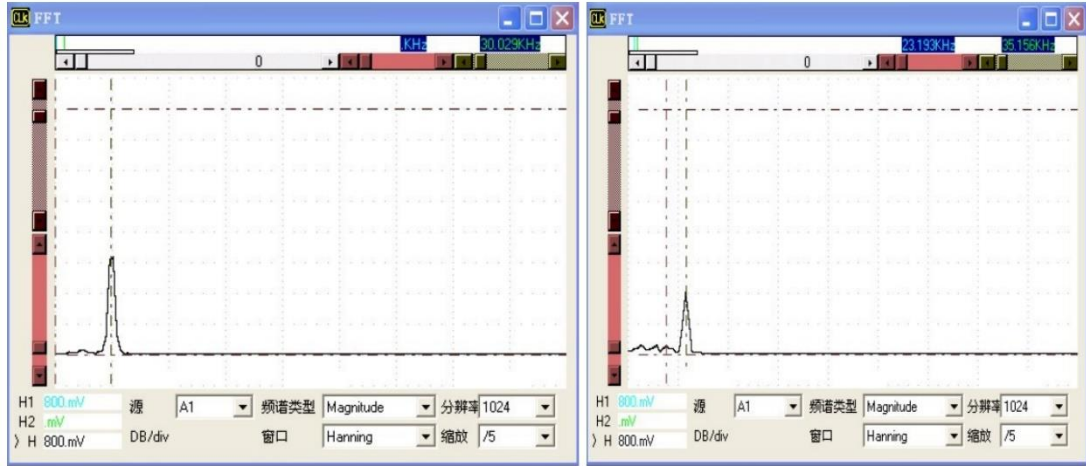


Figure 2.5: The FFT spectrum at (a) 30.039 kHz and (b) 35.156 kHz (Xu et al., 2011)

2.3.3 Fiber Bragg Grating (FBG) Sensors for Acoustic Emission in SHM

Wild and Hinckley have demonstrated the detection of radiation of acoustic waves with the use of FBG sensor. The FBG was designed by varying the refractive index periodically along the core of the SMF.

In FBG, signal transmission only propagates in the fundamental mode and no cladding mode. Hence, the short period grating is represented as a filter during the reflection for wavelength selection, to reflect the signal at certain wavelengths, as illustrated in Figure 2.6. The reflected wavelength is defined as the Bragg wavelength, λ_B is given by (Wild and Hinckley, 2007),

$$\lambda_B = 2n_{eff}\Lambda \quad (2.10)$$

where Λ and n_{eff} are grating period and effective refractive index of fundamental mode respectively. The Bragg wavelength is highly dependent to the elongation of grating imposed mechanically and thermally to the fiber (Rajan, 2015). Therefore, FBG is in general characterized by the Bragg wavelength. Any elongations such as acoustic pressure, temperature, strain and etc. in the FBG will increase the grating period and hence results shifting in Bragg wavelength. Consequently, approximation of the relative changes in Bragg wavelength is shown below (Wild and Hinckley, 2007):

$$\frac{\Delta\lambda_B}{\lambda_B} = C_S S + C_T \Delta T \quad (2.11)$$

where strain, S having coefficient of C_S and ΔT represent the change in temperature with coefficient of temperature, C_T .

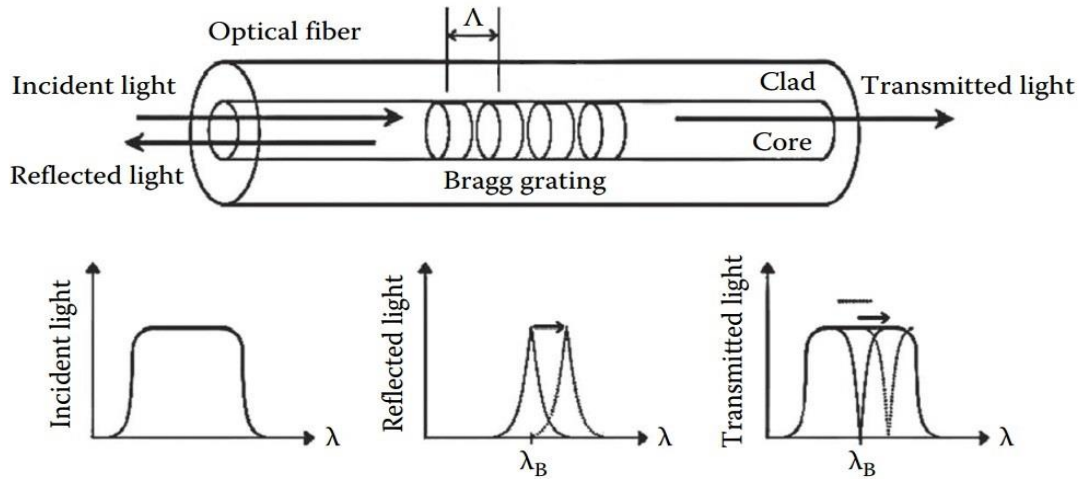


Figure 2.6: Wavelength-selective reflection filter of FBG (Rajan, 2015)

2.3.4 Intensity-Modulated Based Bend Fiber Optic Sensor

Intensity-modulated based bend fiber optic sensor has drawn great attention due to its sensing principle by fully utilizing the undesirable loss (bend loss) and form numbers of applications (Harris and Castle, 1986).

As reported by Nishino et al., a power modulation-based curved waveguide sensor is proposed and developed. The SMF is curved to form a small loop along with measurable intensity losses. This sensor works by allowing the physical perturbation to induce optical intensity losses through curved waveguides i.e. macro-bending. In general, there are various transduction mechanisms to cause the intensity of light change as it propagate through the fiber optic such as macro-bending, fracture, fiber to fiber coupling, modified cladding, absorption, reflectance, molecular scattering, Evanescent fields etc. (Kepak et al., 2013). Among these, the bending loss is important as it formed the fundamental sensing principles for the intensity-modulated based bend fiber sensor. Applied force or displacement that cause random change in the radius of curvature even a slight movement of $1 \mu\text{m}$ will lead to loss in intensity of the propagated light (Gambling and Matsumura, 1978).

Apart from that, the light intensity loss due to macro-bending comprises of two losses which known as transition and pure bend loss. The radiated light is not uniform nor continuous at the beginning of bend, but appears to be discrete divergent rays (Gambling, Matsumura, Ragdale and Sammut, 1978). The coupling of propagated light from the SMF core mode to leaky mode owing to the transform in fiber axis from straight to bend or vice versa (Harris and Castle, 1986). As a result, the light intensity distribution at the onset of bend is oscillate as shown in Figure 2.7 and the oscillatory section is known as the transition region. As the distance along the bend fiber increases, the light beams wider and decreases in amplitude and slowly becomes uniform, thus, the non-oscillate section is known as the pure bend region. In other words, the pure bend loss is caused by the cladding part of the energy associated with the incident core mode, increasing its phase velocity to remain in step with that in the core (Badar and Maclean, 1991).

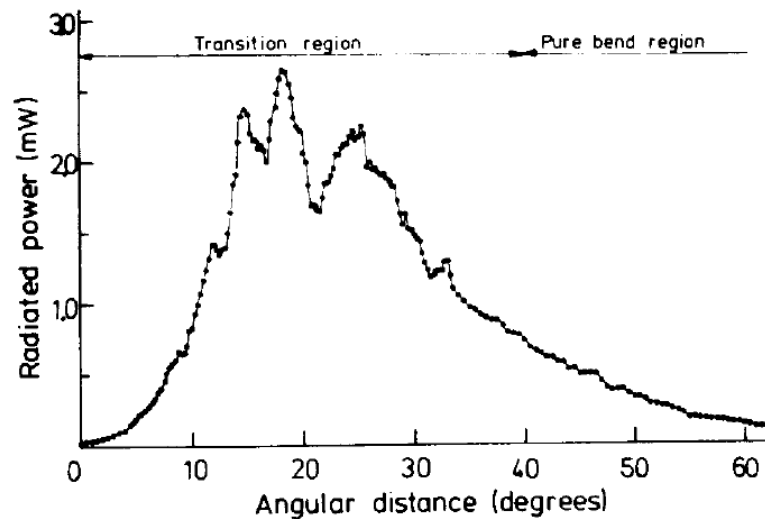


Figure 2.7: The change in light intensity for bend fiber
(Gambling and Matsumura, 1978)

However, not all the radiated light will be permanent loss to the air, there are regions where the light will recoupling back to the core from the leaky cladding modes (Murakami and Tsuchiya, 1978). Therefore, the optical power loss is varied accordingly to the shift in location of the coupling between the core and leaky mode (Nishino, Chen and Gupta, 2014).

According to Nishino et al., the relative output power, P from the fiber optic loop sensor (FOLS) is defined as the ratio of modulated power output, P'_{out} caused

by bending and power output, P_{out} without bending. Figure 2.8 shows the relative output power of the FOLS for radius 6, 7 and 8 mm. The 8 mm FOLS with power drop approximate 20% for 350 μ m displacement is chosen for the rest of the measurements (Nishino, Chen and Gupta, 2014).

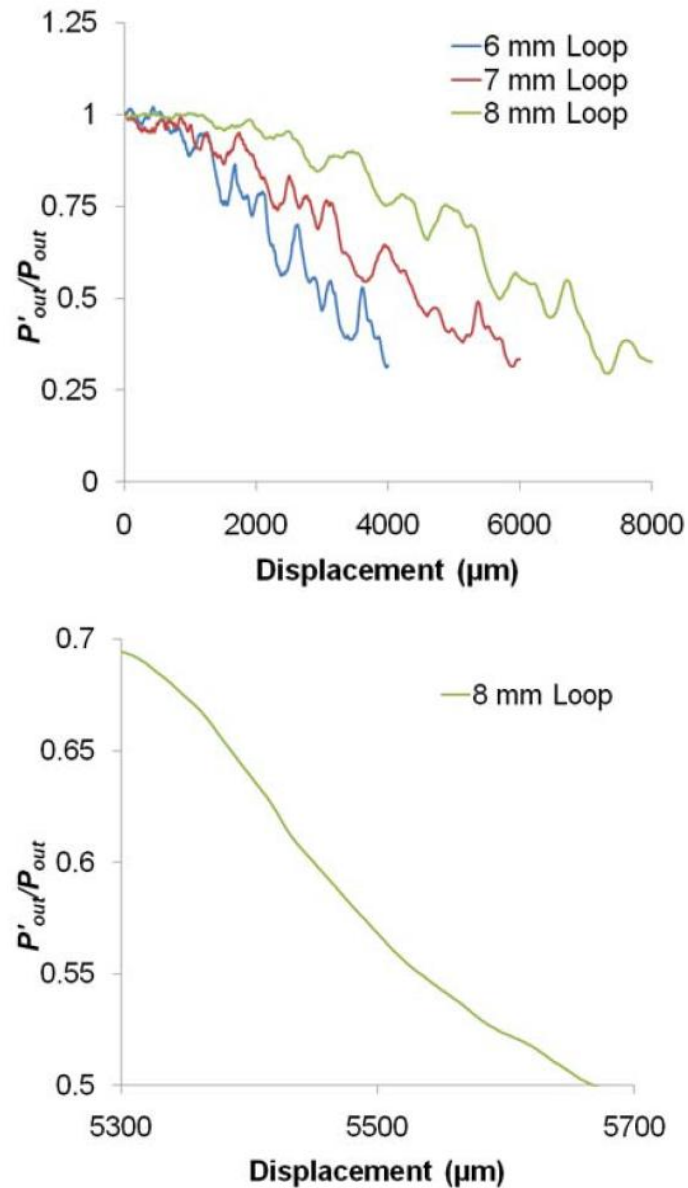


Figure 2.8: Relative output power against displacement for FOLS (6, 7 and 8 mm loop) and the zoom in view for the linear region within one intermediate peak of 8 mm FOLS (Nishino, Chen and Gupta, 2014)

The radiation loss owing to uniform bend increases as the radius of bending decreases. This is due to the changes of refractive index of the fiber. When the fiber

subjected to bending, stress is acting on the internal and outer of the fiber and light transmission at the outer part of the curvature is travelling faster than the inner part which has a smaller inner radius. Hence, the bending of the fiber has affected the light transmission and results in change of optical power (Murakami and Tsuchiya, 1978).

Figure 2.9 illustrated the overall experimental setup for the 8 mm FOLS calibration arrangement. The FOLS is supplied with single-mode laser source at $1310\ \mu\text{m}$ and a small shaker is served as the source of vibration excited by the function generator at frequency 10 and 100 Hz. Results are collected through the photodetector and data acquisition (DAQ) card (PDI 6229 National Instruments) at a sampling rate of 5 kHz.

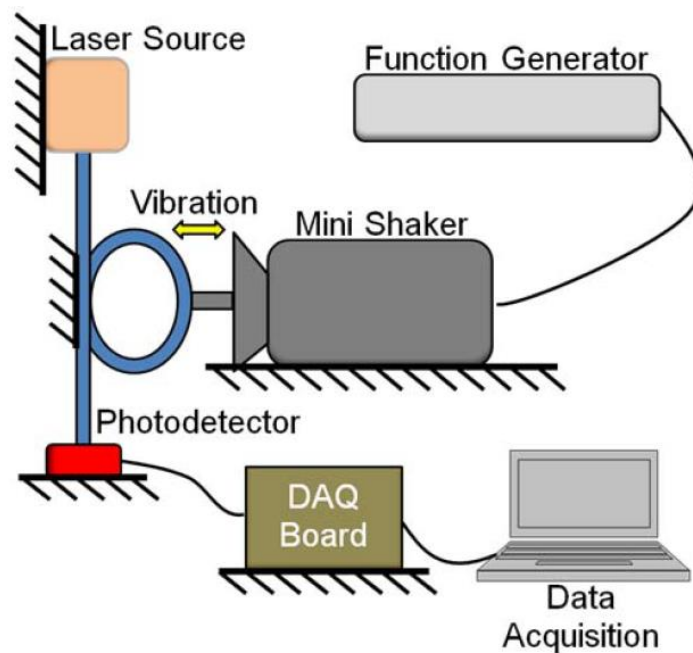


Figure 2.9: Experimental setup of FOLS calibration arrangement
(Nishino, Chen and Gupta, 2014)

The results presented in Figure 2.10 shows the frequency response of the FOLS and confirms the measured vibration frequency with a sharp peak corresponding to 10 and 100 Hz depicted in the figure. However, for vibration frequency of 10 Hz, resonance peaks are captured along with the fundamental peak owing to the mode of windowing in FFT and leakage of spectral (Nishino, Chen and Gupta, 2014).

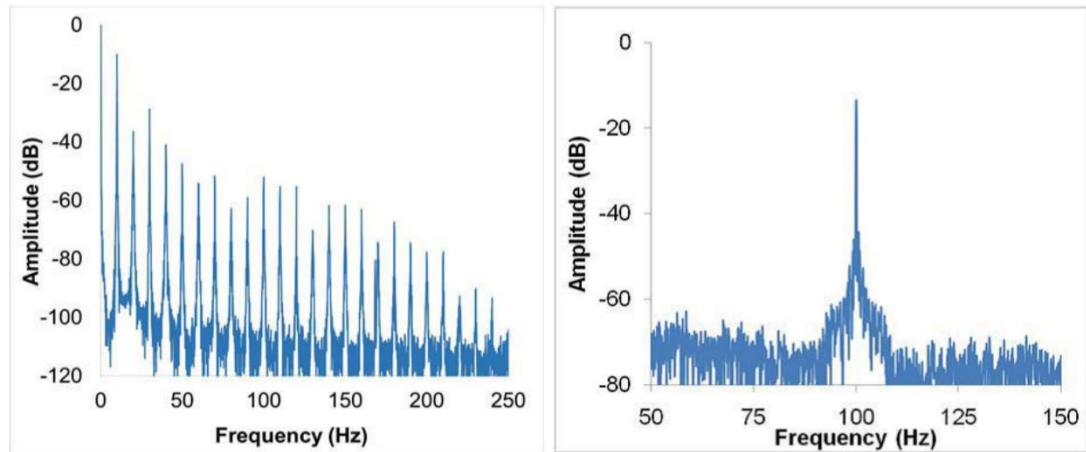


Figure 2.10: Frequency response of FOLS at 10 and 100 Hz (Nishino, Chen and Gupta, 2014)

2.4 Comparison of FOSs

After classified the criterion of the optical fiber sensors aforesaid, the fabrication methods, merits and limitations of these sensors are abridged in Table 2.1.

Table 2.1: Evaluation of types of FOS

Sensor	Fabrication Methods	Merits	Limitations
Single Taper Fiber	<ul style="list-style-type: none"> • Flame heating • Fiber pulling • Laser ablation 	<ul style="list-style-type: none"> • Insensitivity to temperature changes. • No requirement for coherence properties of light source. 	<ul style="list-style-type: none"> • Fragile at tapered segment.
SMS Fiber	<ul style="list-style-type: none"> • Fusion Splicing 	<ul style="list-style-type: none"> • No feedback control loop. • Wide area detection • Low power consumption 	<ul style="list-style-type: none"> • Complex multimode radiation pattern. • Difficulties in demodulation of wanted information
FBG	<ul style="list-style-type: none"> • UV irradiation • Electron beam interference lithography 	<ul style="list-style-type: none"> • High resolution • Multiplexing capability 	<ul style="list-style-type: none"> • Fragile • Cross sensitivity to humidity and temperature (Rajan, 2015)

Table 2.1 (Continued)

FOLS	<ul style="list-style-type: none"> • Macro-bending 	<ul style="list-style-type: none"> • Considerable high resistance to stretch or compress • Ease of fabrication • Low cost 	<ul style="list-style-type: none"> • Cross-sensitivity to vibrations
-------------	---	--	---

2.5 Design of Bend Coated Fiber Sensor

The fiber optic sensor based on macro-bending is chosen to be justified by carries out further acoustic vibration calibrations. As bend coated fiber optic sensor offer a number of advantages with compared to other well-established optical fiber sensor (e.g. interferometer) in SHM applications. For instance, the incredible simplicity of configuration allows the use of ordinary optoelectronic devices. In addition, it also capable to provide relatively high measurand sensitivity and shows considerable high resistance to stretch or compress by the applied loads. In the following section, the optimum design criterion of bend coated sensor is demonstrated.

2.5.1 Fabrication Criteria

As reported by Shahami, the optimum parameters for the bend radius, wrapping turn number, numerical aperture, NA of fiber and the critical radius of bending is shown in Table 2.2 below (Shahami, Siti Azlida and Dambul, 2016).

Table 2.2: Optimum parameters for the bend loss sensor (Shahami, Siti Azlida and Dambul, 2016)

Optimum Parameters	
Bend radii	5.5 mm
Wrapping turn	1 to 5 turns
Numerical aperture	0.2
Critical radius	5 to 13 mm

CHAPTER 3

METHODOLOGY AND WORK PLAN

3.1 Introduction

The process of fabrication, packaging and measurement system, including the bend coated fiber sensor will be demonstrated and present in this chapter. Furthermore, the implementation of the fiber sensor in field test will be discussed as well. Figure 3.1 below shows the overall work flow of this project in chart.

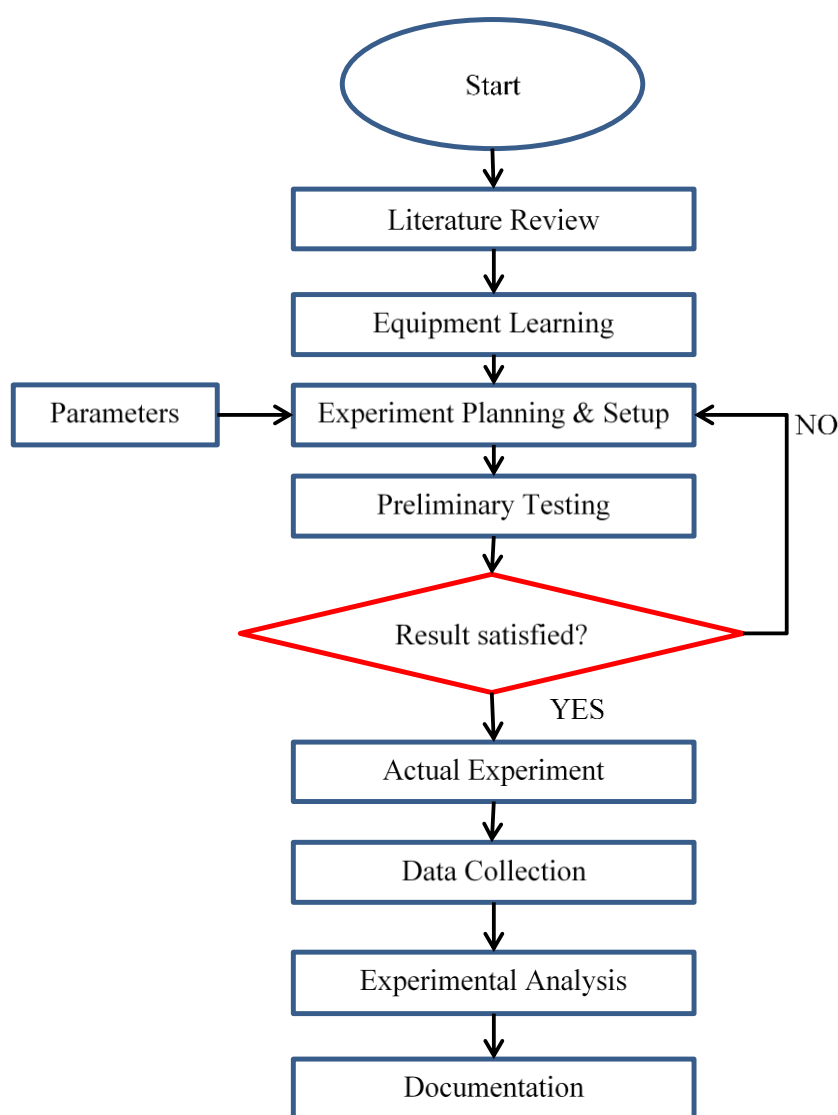


Figure 3.1: Flow chart for overall project of acoustic vibration fiber sensor for pipeline leakage detection

3.2 Flow Chart of the Work Plan

Figure 3.2 illustrates an overview of the work plan in carry out the research study, fabrication, packaging and characterization of bend coated fiber sensor. Details for the implementation of each blocks will be discussed in next section.

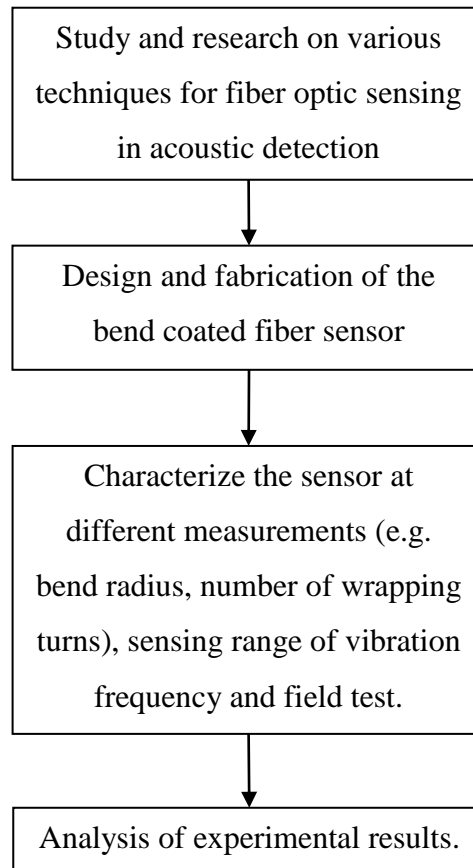


Figure 3.2: The work plan for the development of bend coated fiber sensor

3.3 Design and Fabrication of Sensor

The implementation of each of the blocks shown in Figure 3.2 is discussed in this section. For the first block, study and research on various techniques for fiber optic sensing in acoustic vibration have already been discussed in previous Chapter 2. Therefore, this section focus on the discussion of design, fabrication and the characterization of the fiber sensor.

3.3.1 Design of Sensor

In this project, the SMF fiber is used as the sensor for detection. Figure 3.3 depicted the ring design of the fiber sensor. The sensor configuration is extremely simple, which consist of a bending loop and hold by the adhesive tape. The bending loop acts as the sensing arm to detect the perturbation (i.e. vibration).



Figure 3.3: Configuration of the bend-coated fiber sensor

3.3.2 Fabrication of Sensor

The fabrication of macro-bend fiber sensor comprise of few processes that included stripping of polymer coating of SMF at two ends, cleave the core of the fiber to ensure that the cutting edge of the fiber is flat and finally the SMF is spliced with the pigtails using the Sumitomo Fusion Splicer as illustrated in Figure 3.4.



Figure 3.4: The Sumitomo fusion splicer and cleaver

Once these processes have been done the SMF will be configured by bending the fiber to form a ring in free space and the intersection of the SMF is taped by adhesive tape to hold the loop.

3.4 Characterisation of Sensor

The fiber used in this project is SMF-28 fiber manufacture by Corning with mode field diameter $10.4 \pm 0.5 \mu\text{m}$ at $1.55 \mu\text{m}$, clad diameter $125 \pm 0.7 \mu\text{m}$ and core diameter $8.2 \pm 5 \mu\text{m}$ given by Corning SMF-28 datasheet as shown in Appendix B. Before the bend coated fiber sensor is implemented in acoustic vibration and field test (water pipeline), it has been characterized by measuring the bending loss on various bending radius (5 to 16 mm) and different number of wrapping turns, N .

The equipment for the measurement of bend loss in fiber optic is illustrated in Figure 3.5. In this setup, it consists of a single wavelength laser source which is able to produce light source at 1310 nm, 1490 nm and 1550 nm wavelength and a power meter which used for measuring the output optical power loss (dB). However, only the C-band wavelength (1550 nm) will be used in the entire project.



Figure 3.5: Bending loss measurement setup

3.4.1 Measurement of Losses on Various Bend Radius

In order to measure the losses caused by bending, both ends of the fiber with connector is connected to a laser source and optical power meter. It is worth mention that before starting to measure the bending loss, without bending the fiber and the

optical power meter is calibrated to the reference value at 0.00 dB as shown in Figure 3.6.



Figure 3.6: The reference value of the optical power meter is set to 0.00 dB

Hereafter, the fiber is bent to various radius (5 to 16 mm) and the adhesive tape is used to hold the loop. Power losses are observed from the power meter as illustrated in Figure 3.7 and these values are recorded according to bend radius respectively.



Figure 3.7: Losses display on the power meter due to the bending of fiber

3.4.2 Measurement of Losses on Various Wrapping Turns

To observe the impacts of different wrapping turns, N (up to 10 turns) of fiber with bend radius 8, 10 and 12 mm. Owing to the number of turns, a mandrel (cylindrical rod) of different diameters are used to make sure each turn is at the same diameter.

The arrangement of the measurement setup is shown in Figure 3.8. The setting of the power meter is same as the previous section.

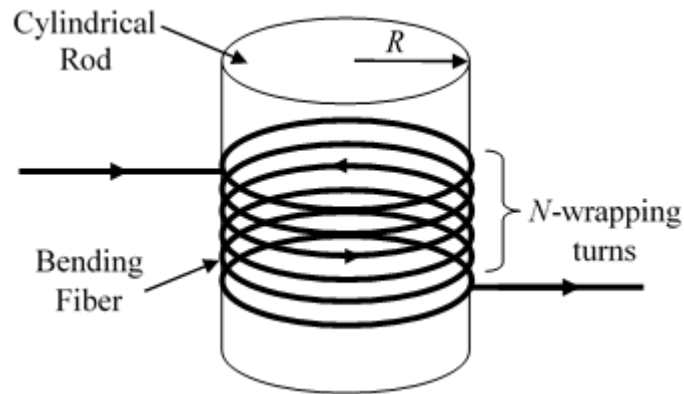


Figure 3.8: The setup for measuring bend loss at different number of wrapping turns on a mandrel

3.5 Implementation of Sensor in Acoustic Vibration Test

The experimental setup for the acoustic vibration test is constructed as shown in Figure 3.9. The bend coated fiber sensor is attached on a square polypropylene plate. The polypropylene plate is used to serve as a platform to hold the position of the fiber sensor.

A commercial speaker is emulated as the acoustic vibration source used to produce constant frequency and amplitude vibration based on the setting of the signal generator. This speaker is placed underneath the plate in which the sensor is attached.

Laser source with wavelength 1550 nm is injected to the fiber sensor, and the other end where the output optical power is connected to a photo-detector. These optical signals are then converted into electronic signals displayed through the oscilloscope. In addition, the signal in time domain is converted into frequency domain through FFT and the background noise is filtered through notch filter.

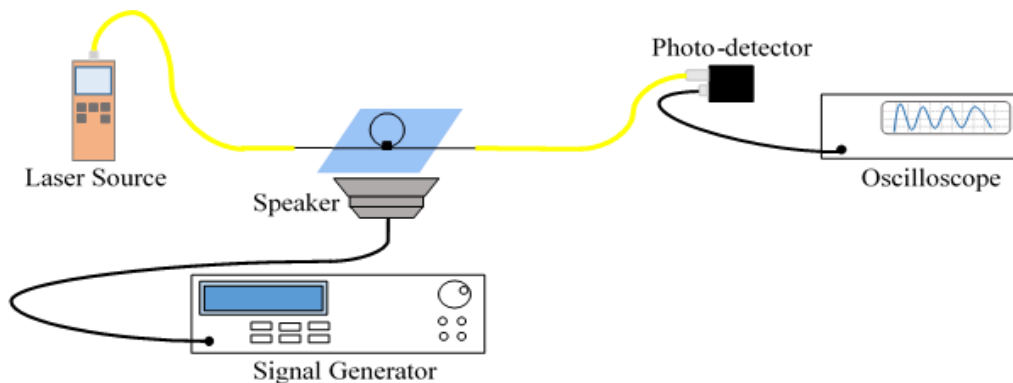


Figure 3.9: Experimental setup for acoustic vibration test

In this test, vibration frequency produce is mainly focused on low frequency from 20 Hz to 3000 Hz as the aim of this project is to develop a fiber sensor for low frequency acoustic vibration detection.

3.6 Implementation of Sensor in Field Test (Water Pipeline)

Once the fiber sensor is characterized in term of bend radius and sensing range for vibration frequency, it will be implemented in the field test for further investigation the applicability of the sensor in real life application. The pressure for these pipeline line is low

For the field test depicted in Figure 3.10, the overall experimental setup is same as in the vibration test. But in field test, the bend coated fiber sensor is attached on the surface of the pipe wall using adhesive tape. Aside from that, an iron block is placed on top of the bend coated fiber sensor in order to achieve better coupling between the acoustic wave generated from the leak hole and the fiber sensor.

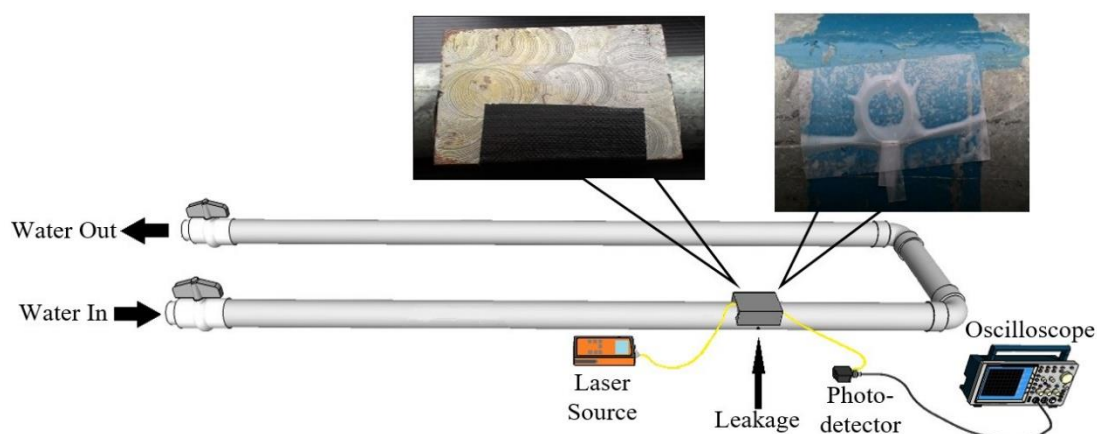


Figure 3.10: Experimental setup for the field test

CHAPTER 4

RESULTS AND DISCUSSIONS

4.1 Bending Loss Measurements

In the part hereof, the bending loss and its variation for bend coated fiber sensor will be measured and characterized. The influence of the bend radius, R on the losses of bend coated fiber sensor was investigated and also the impacts of number of wrapping turns, N to the bend loss was studied. These consequences due to different bend radius and wrapping turns of the bend coated fiber sensor will be elaborated in details in the following sections.

4.1.1 Bend Radius Dependent Property of the Sensor

So as to determine the range of bending radius for characterization, the minimum critical bend radius of SMF with negligible loss is obtained at approximate $R_c \approx 16$ mm from the equation (4.1) reported by (Zhang and Ball, 2001). The calculation is shown in Appendix A.

$$R_c \approx \frac{20\lambda}{\sqrt[3]{\Delta_n}} \left[2.748 - 0.996 \left(\frac{\lambda}{\lambda_c} \right) \right]^{-3} \quad (4.1)$$

where λ and λ_c are the operating wavelength and cut-off wavelength respectively. For the relative difference of refractive index, Δ_n is given by equation (4.2):

$$\Delta_n \approx \frac{NA^2}{2n_1} \quad (4.2)$$

where NA and n_1 are the numerical aperture and refractive index for fiber core stated in Table 4.1 obtained from Corning SMF-28 datasheet shown in Appendix B.

Table 4.1: Parameters of Corning SMF-28 fiber at wavelength 1550 nm

Parameters	Unit(s)	Core	Cladding
RI		1.4682	1.4629
Radius	μm	41.5	62.5
NA		0.13	

As a result, the optical fiber is choose to bend at different radius ranging from 5 to 16 mm at the operating wavelength of 1550 nm. The reason is when the radius of the curvature is bend greater than the critical value of the fiber is insensitive to the macro-bending. The photons in the propagated bend light wave move on circular paths concentric with the axis of bending (Neumann, 2013). As, if the bend radius is reduced below the critical value, the bend loss will increase rapidly due to the phase velocity of the outer part of fiber are equal and cannot be greater than the velocity of light in the cladding. This allow the construction of a relatively sensitive bending fiber sensor (Hu and Huang, 2009).

However, the experiment has stopped at bend radius, R less than 5 mm owing to exceedingly too high of bending loss in the fiber. Secondly, this is to avoid the incidence of micro-cracks in optical fiber, especially in very low radius of curvature, which will affect the fiber performance.

The variation of the bend loss counter to the radius of curvature is illustrated in Figure 4.1.

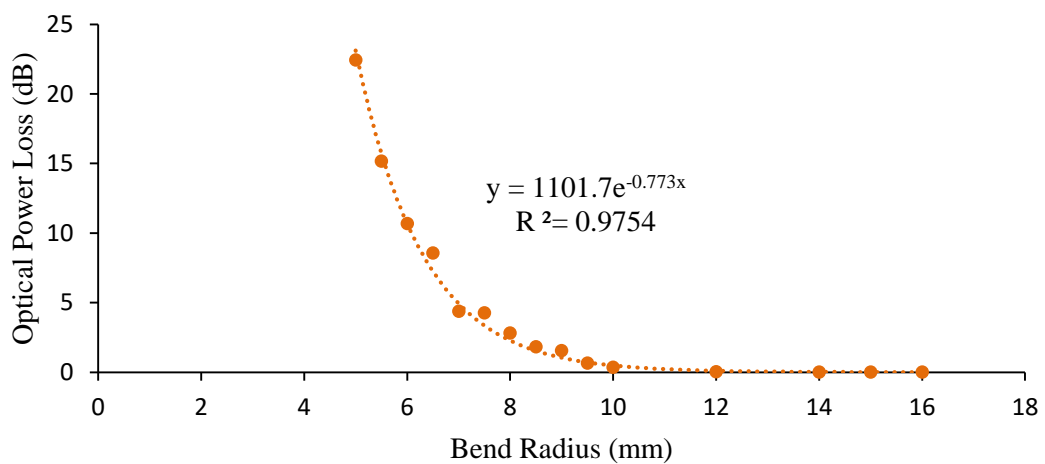


Figure 4.1: Relationship between the bend loss and correspond bend radius at 1550 nm wavelength

Based on the results depicted in Figure 4.1, the power loss for bend radius greater than 10 mm is very small and almost negligible due to the low bend loss value of the SMF-28 (Wang et al., 2010). When the bend radius of the fiber decreases gradually less than 8 mm, the optical power loss increase significantly from -2.82 dB to -22.44 dB. Hence, this particular bend radius will be choose as the threshold bend radius for the fiber sensor. Consequently, the sensitivities of the fiber sensor will be characterized with bend radius right after the threshold value.

Furthermore, for each bend radii the bending loss was measured and recorded. It can be observed from the result that high bending loss will be induced for smaller bend radii. To formulate the losses, the measured bending loss in this experimental at different bend radii are fit into the equation (4.3):

$$L_R = \xi_1 \exp(-\xi_2 R) \quad (4.3)$$

where L_R is the bending loss for various bend radii while ξ_1 and ξ_2 are fitting parameters. Such fitting values are added for comparison with the experimental results. The fitting curve shows good agreement with the measured bending loss. In other words, the simplified formula can be used to estimate the bending loss for the bend coated fiber sensor at various bend radius. Also, this equation is proved for fast calculation and feedback control in the quality checking systems reported by Tsao and Cheng (Tsao and Cheng, 2002).

4.1.2 Number of Wrapping Turns Dependent Property of the Sensor

In this section, impacts of wrapping turn, N on the bending loss is considered. The variation of bending loss against the number of wrapping turns ($N = 10$) for bend radius, R of 8, 10, and 12 mm is shown in Figure 4.2.

Obviously from the experimental results, a linear relationship between the bending loss and wrapping turns is obtained for the bend radius 8, 10 and 12 mm. Besides, the gradient of these lines are much depending on the bend radius of the fiber. For the experimental results, a linear equation (4.4) can be used to satisfy the results (Tsao and Cheng, 2002):

$$L_N = \xi_N N \quad (4.4)$$

where L_N is the bending loss for different wrapping turns and ξ_N is the fitting parameter due to wrapping turns. Consequently, by increasing the number of wrapping turns, N the power loss increases and achieves higher bend loss in spite of the value of the bend radius is larger. This property provides great flexibility to the bend coated fiber sensor in term of bend radius as the same losses could be achieved by just increasing the number of wrapping turns.

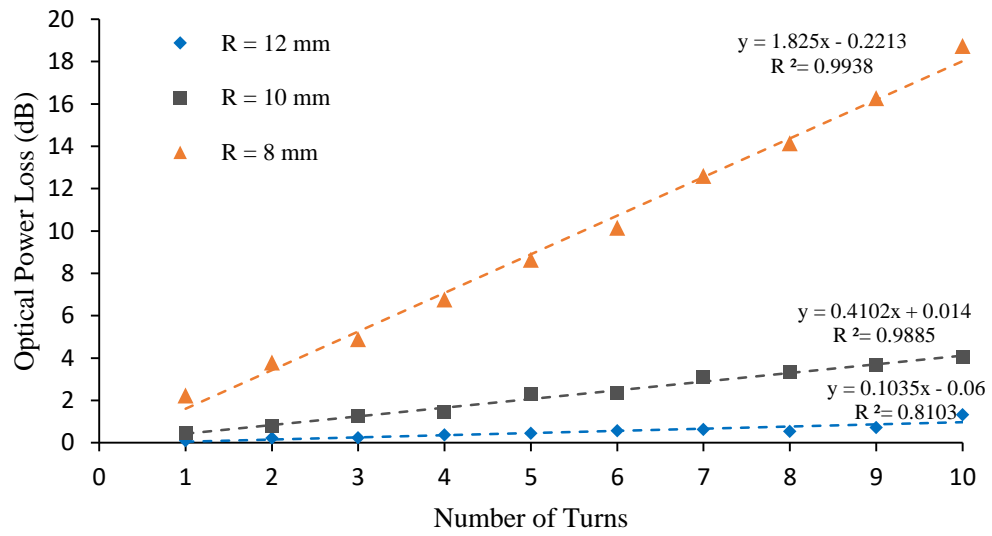


Figure 4.2: The relationship of power loss against wrapping turns, N for bend radius, R equals to 8, 10, and 12 mm

In addition, variation of bend radius and wrapping turns counter to the bending loss is illustrated in Figure 4.3. Surface plot is used to visualize the inter-relationship between these variables. Clearly, when the bending radius and wrapping turns increases, the power loss increases as well. However, more number of wrapping turns are needed for larger bend radius to achieve the same losses experience by smaller bend radius.

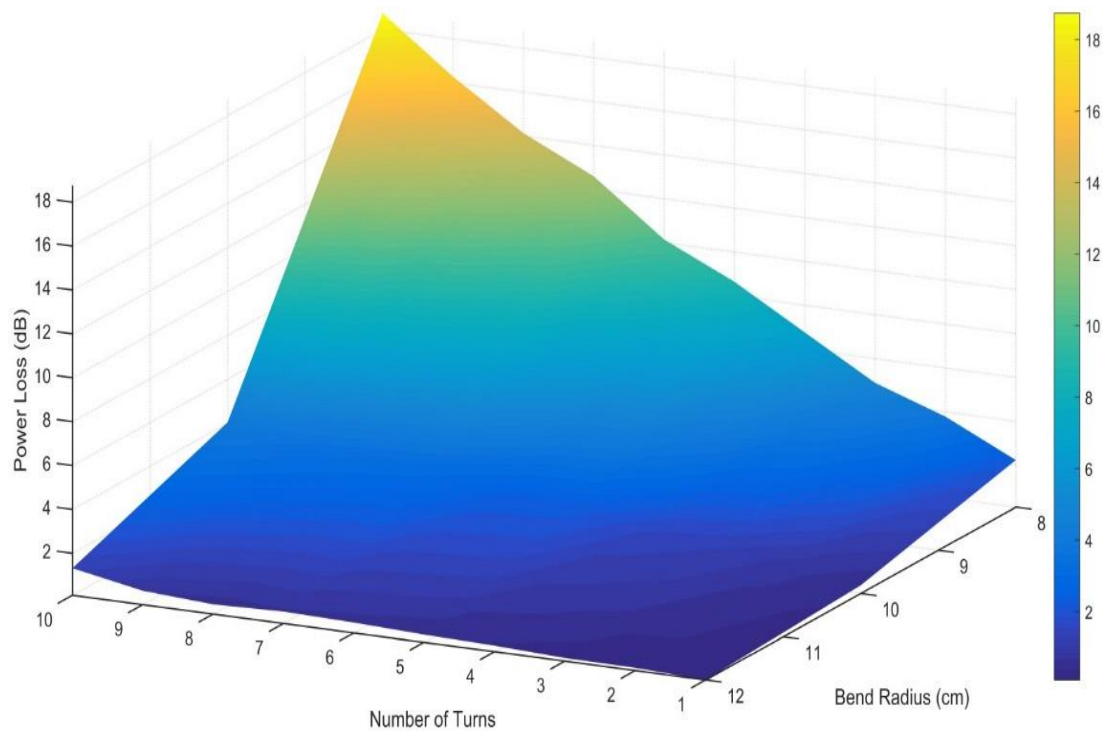


Figure 4.3: The inter-relationship between the bend radius and wrapping turns against the bending loss

4.2 Acoustic Vibration Test

Acoustic vibration detection of low frequency of the bend coated fiber sensor is an important criterion to be characterized in this project. The bend radius of the curvature was expected intuitively affects the sensitivity of sensor, in term of the optical power loss is varied accordingly to the shift in location of the coupling between the core and leaky mode (Nishino, Chen and Gupta, 2014). Various bend radius is used in order to differentiate the sensing range of the bend coated fiber sensor in low frequency.

In the acoustic vibration test, the fiber sensor is bent smaller than the threshold (< 8.0 mm) as aforesaid with bend radius of 2.5, 5.0 and 7.5 mm as illustrated in Figure 4.4.

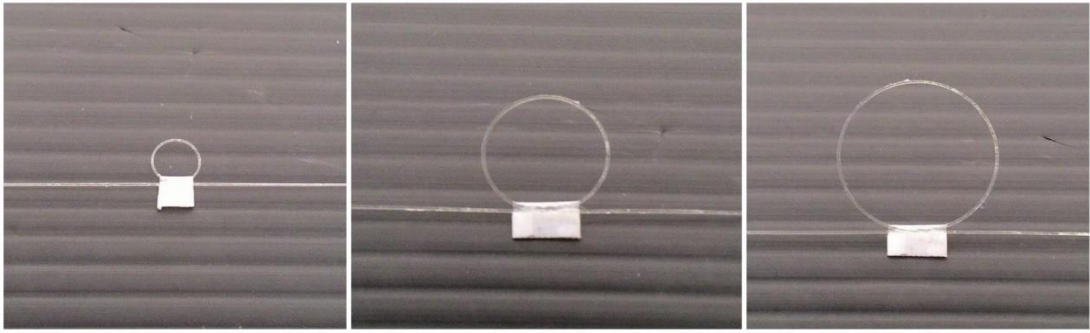


Figure 4.4: The bend coated fiber sensor with bending radius of 2.5, 5.0 and 7.5 mm

Owing to the bending loss is too small and almost negligible for radius greater than critical bend, hence, will lead to inaccurate measurements. Then, a commercial speaker is used to emulate the acoustic vibration source and applied to the fiber sensor. The time domain signal is captured and converted into frequency spectrum through FFT. Also, the unwanted noises or interferences are filtered through notch filter.

4.2.1 Background Signal

Figure 4.5 shows the background profile of the fiber sensor at different stages of signal processing. After the electrical interference with fundamental frequency of 50 Hz is filtered through the notch filter, then, these signals is smoothen by enveloping and averaging. Same signal processing techniques are implemented in both acoustic vibration test and field test. The background signals are collected for the fiber sensor without applying any vibration to the bending segment (i.e. sensing arm). These background signals are similar for the fiber sensor with radius of 2.5, 5.0 and 7.5 mm. The background pattern clearly shows that there is no dominant peak along the frequency domain from 0 to 1000 Hz when no vibration is exerted to the sensor. Therefore, this indicates that the background pattern of the bend coated fiber sensor can be used as the benchmark to observe the external modulation effect.

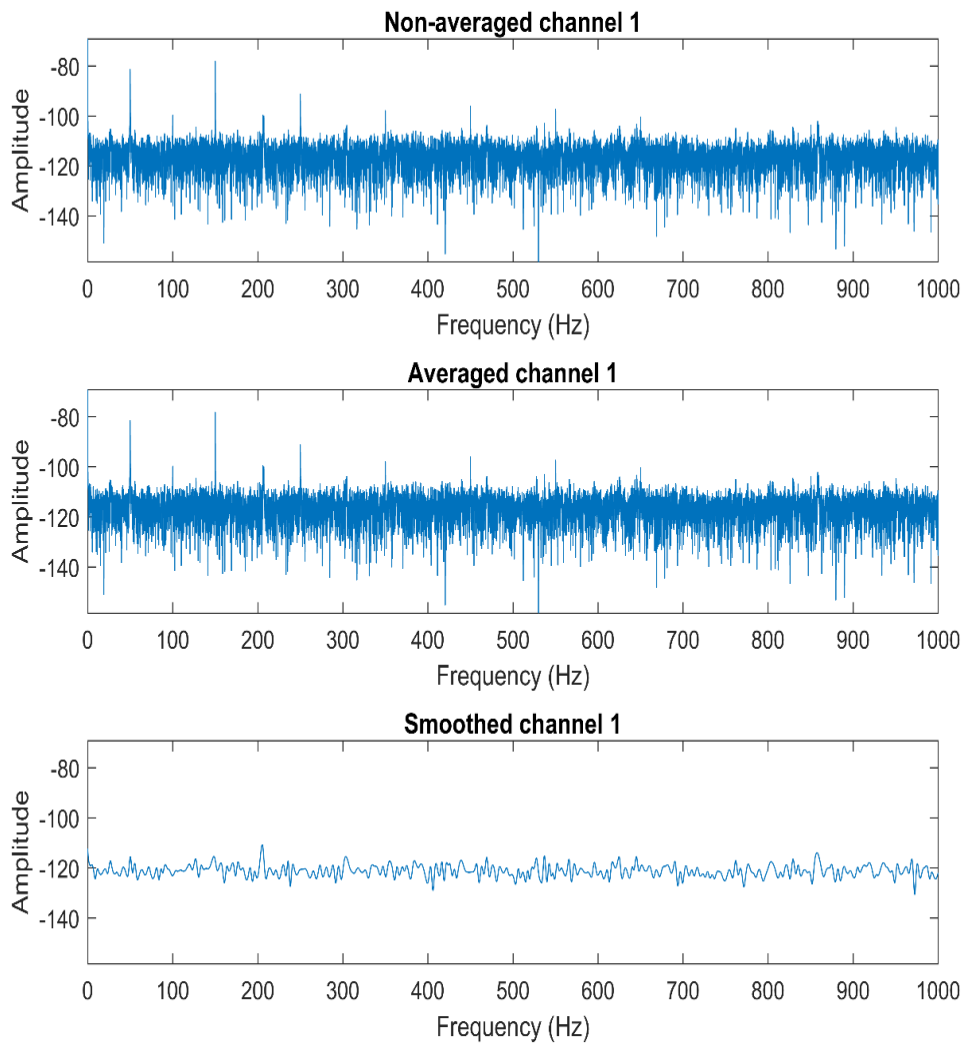


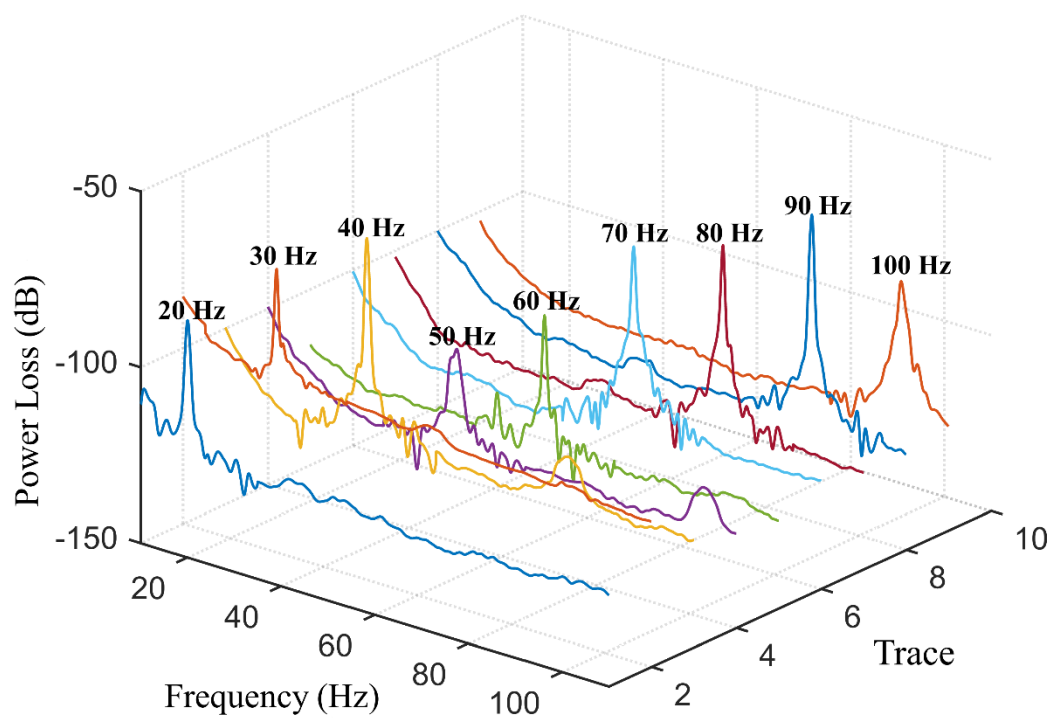
Figure 4.5: The background signal of the fiber sensor from 0 to 1000 Hz

4.2.2 Acoustic Vibration Signals

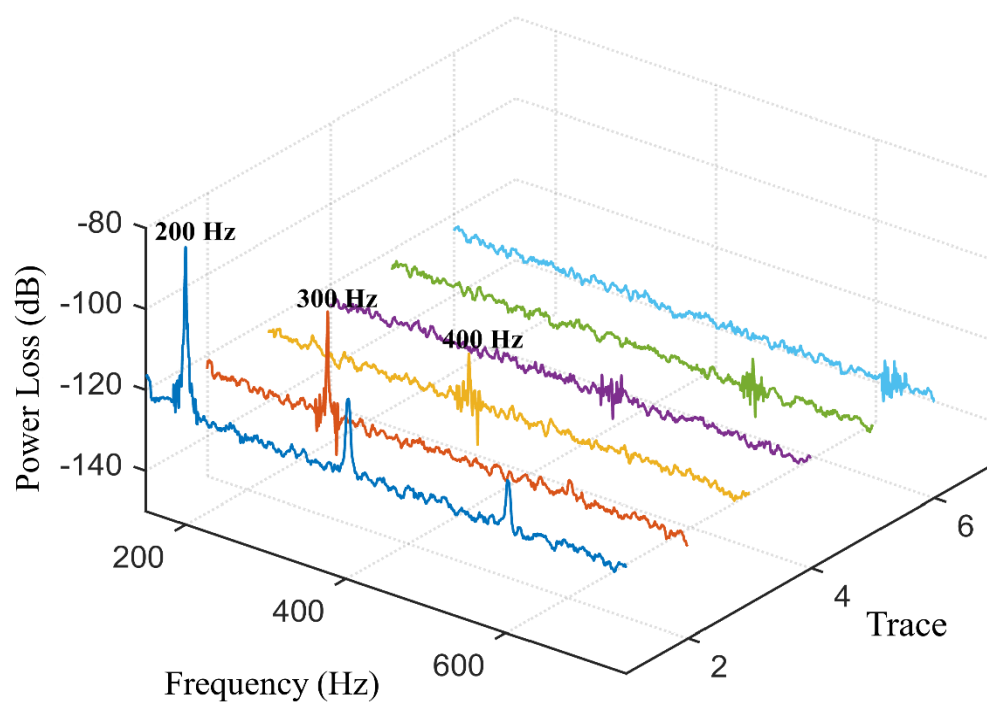
Insets Figure 4.6, 4.7 and 4.8 shows the recorded frequency response of the bend coated fiber sensor with bend radius of 2.5, 5.0 and 7.5 mm. The acoustic vibration is produced by the speaker as aforementioned with vibration frequency varies from 20 Hz to 3000 Hz. Table 4.2 shows the increment for each frequency range.

Table 4.2: The increment of intervals for the frequency range

Frequency Range	20 to 100 Hz	100 to 1000 Hz	1000 to 3000 Hz
Increment	10 Hz	100 Hz	200 Hz



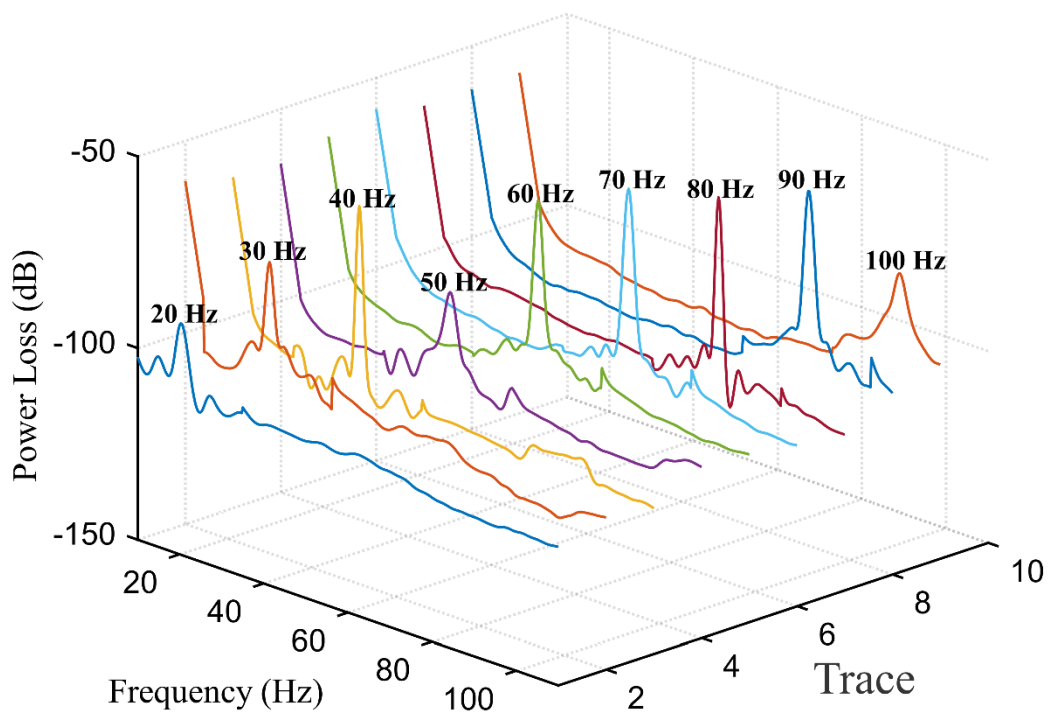
(a)



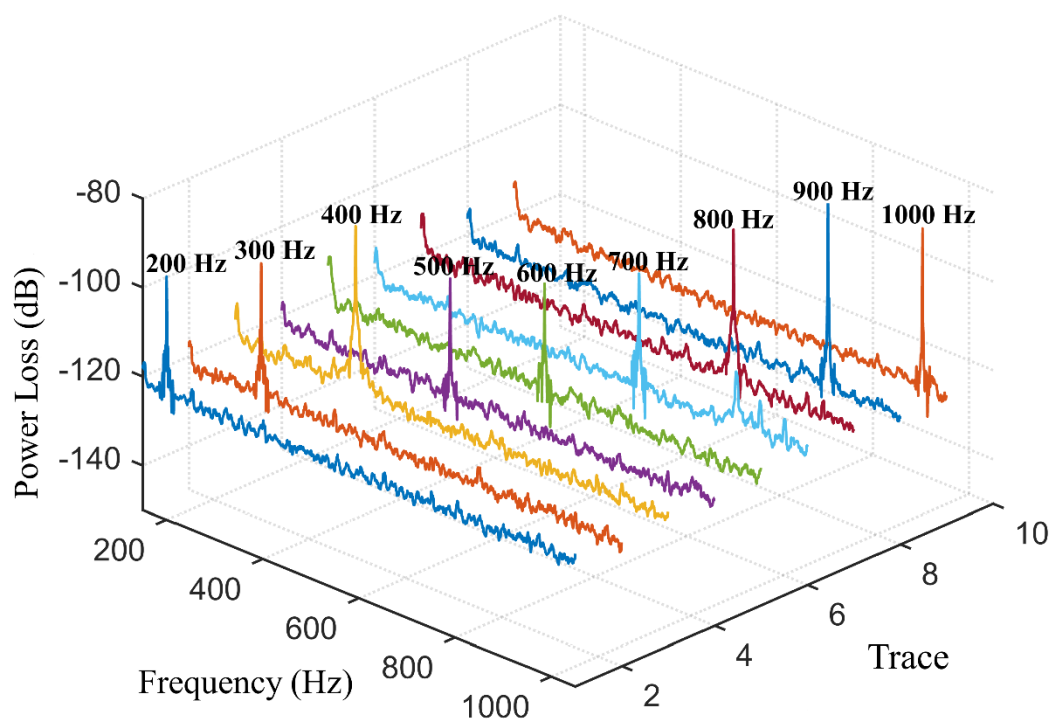
(b)

Figure 4.6: Frequency response of 2.5 mm sensor at frequency range of (a) 20 Hz to 100 Hz & (b) 200 Hz to 600 Hz

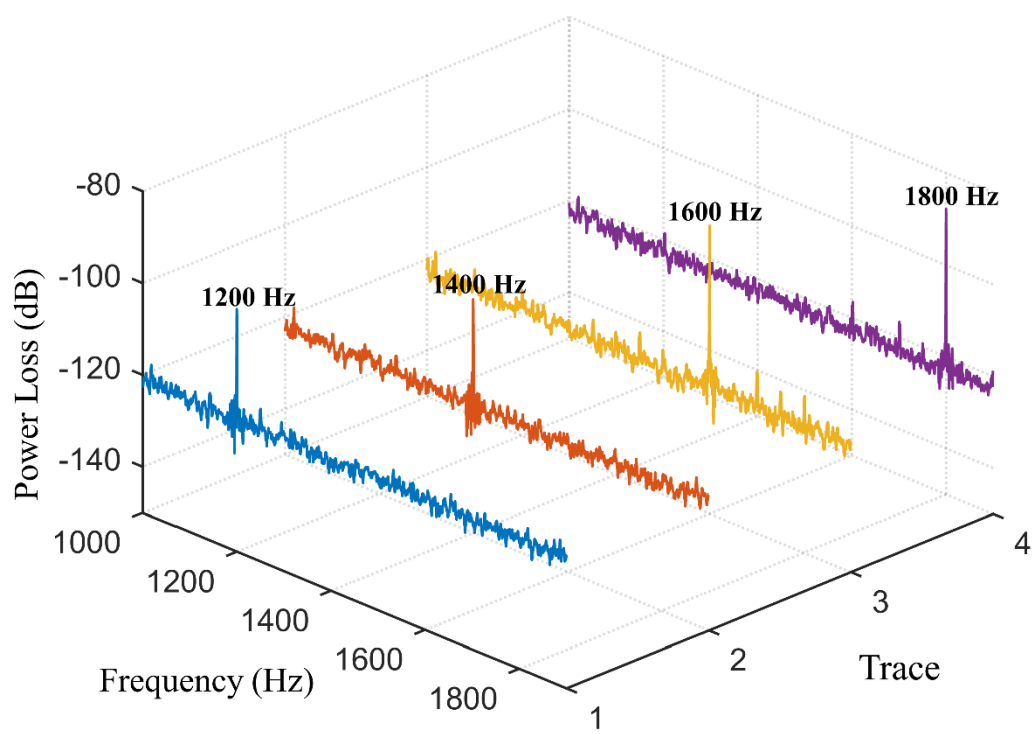
From the results, a common phenomenon shown in the frequency response of the bend coated fiber sensor in which the shifting of dominant peak frequency correspond to the vibration frequency generated by the speaker. For instance, the 20 Hz peak frequency in Figure 4.6 (a) shift constantly to 100 Hz as the vibration frequency increases at the 10 Hz per increment. Furthermore, it is noticed that the corresponding harmonics are detected owing to the induced vibration frequency. This is caused by the slightly non-axial alignment between the vibration source and sensing segment of the bend coated fiber sensor (Huang, Guo, Lu and Tam, 2010).



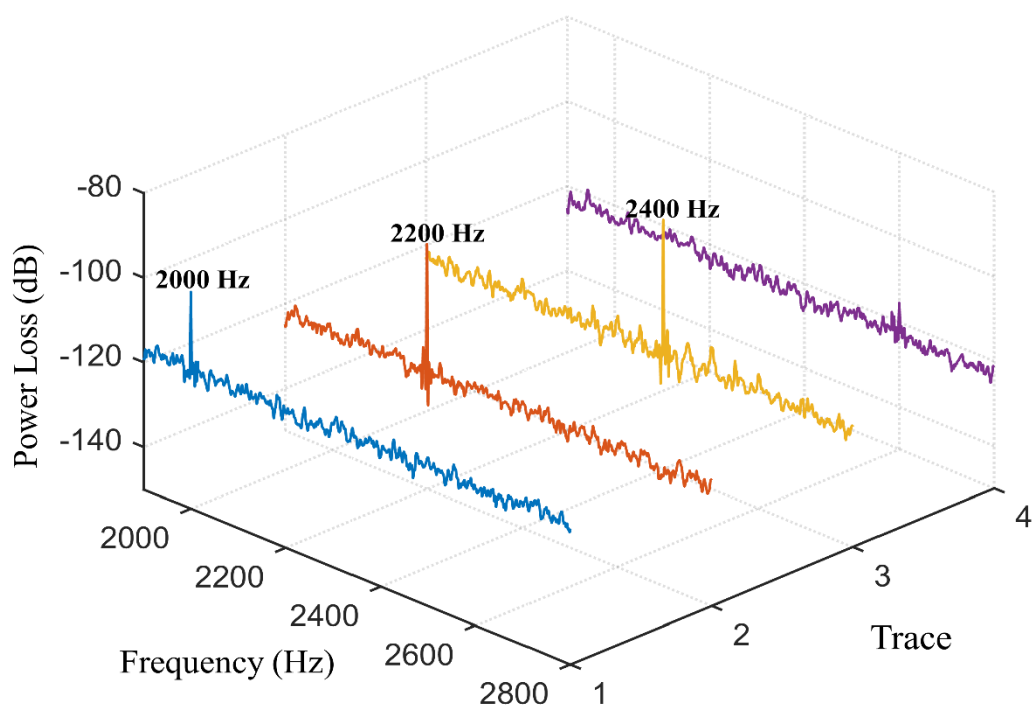
(a)



(b)

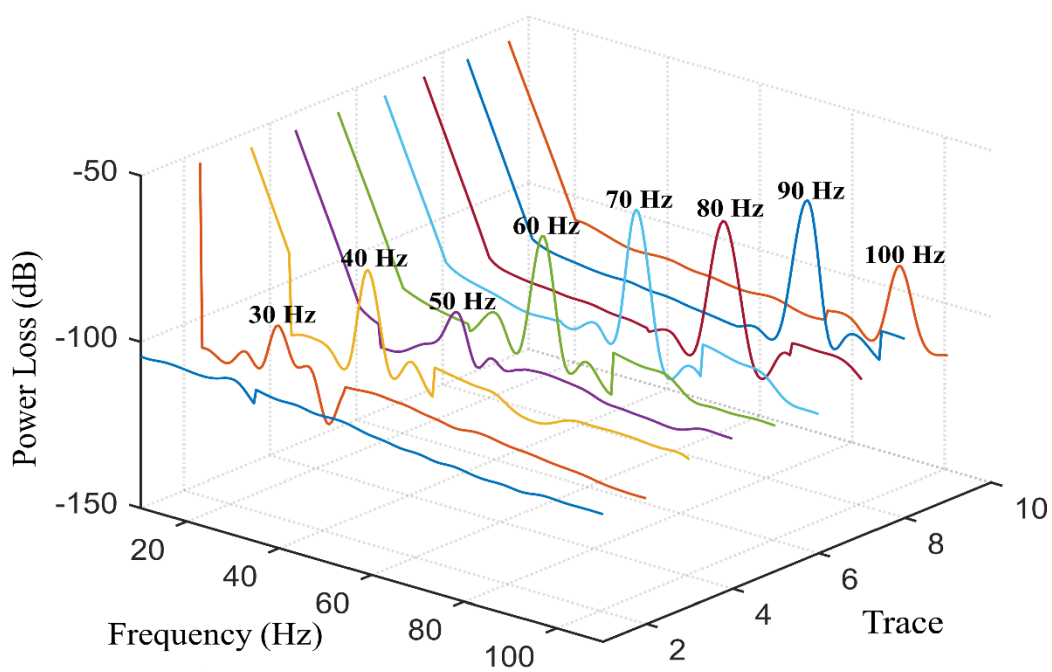


(c)

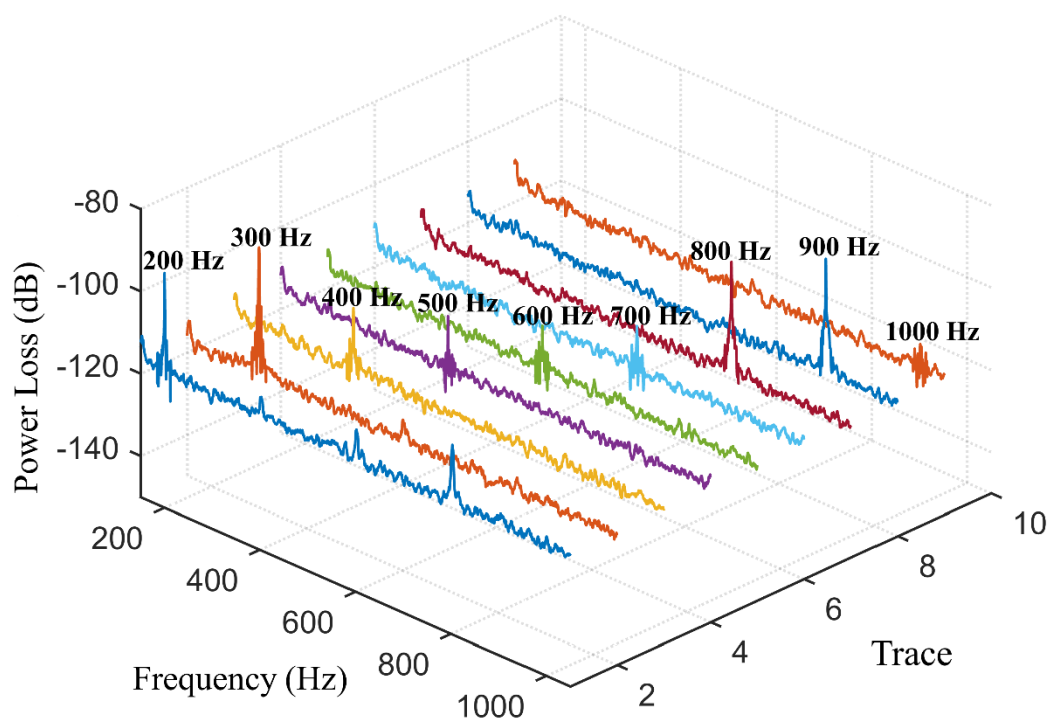


(d)

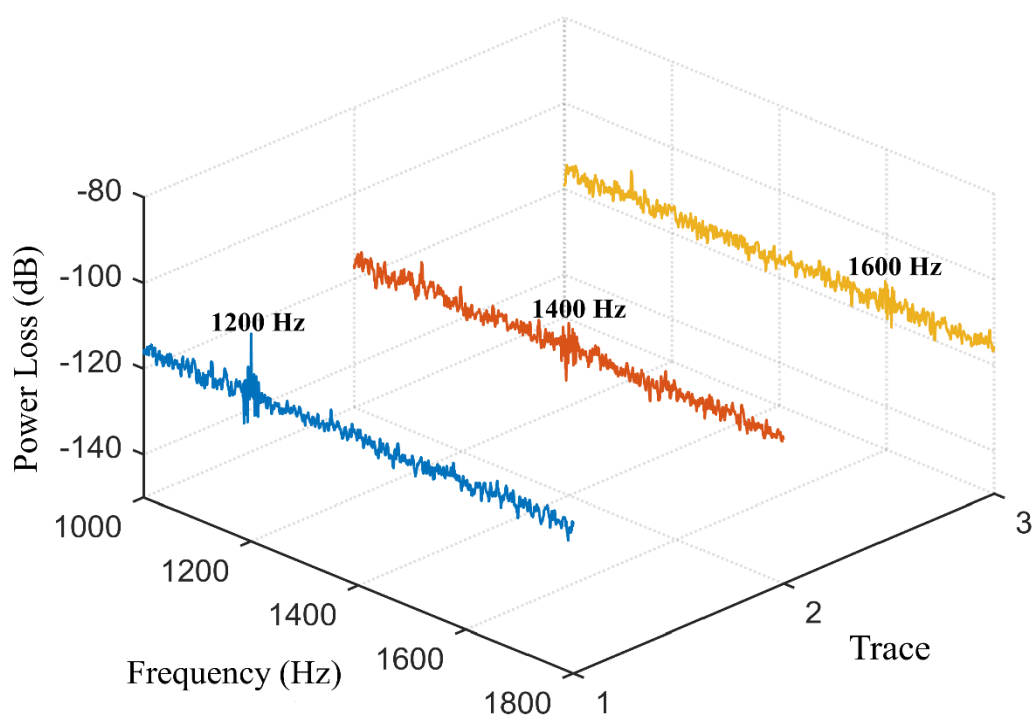
Figure 4.7: Frequency response of 5.0 mm sensor at frequency range of (a) 20 Hz to 100 Hz (b) 200 Hz to 1000 Hz (c) 1000 Hz to 1800 Hz & (d) 2000 Hz to 2600 Hz



(a)



(b)



(c)

Figure 4.8 : Frequency response of 7.5 mm sensor at frequency range of (a) 20 Hz to 100 Hz (b) 200 Hz to 1000 Hz & (c) 1000 Hz to 1600 Hz

The peak frequency of the demodulated response shows a sharp spike which allows distinct identification of the induced vibration frequency. Based on the results, fiber sensor with bend radius of 5.0 mm shows the widest detection range from 20 Hz to 2500 Hz as compared to bend radius of 7.5 and 2.5 mm. However, the 2500 Hz is not shown in the Figure 4.7 (d) as the increment between each interval for frequency range from 1000 to 3000 Hz is 200 Hz aforementioned.

For bend radius equal to 7.5 mm, it only able to detect vibration started from 30 Hz to 1200 Hz. The SNR at 600, 700 and 1000 Hz is likely to be too low in average with approximate to -107.9 dB. This may cause difficulty to distinguish between the signal and noise. As the vibration continues increases to 1400 Hz and 1600 Hz the dominant peak totally diminished. This shows the fiber sensor unable to detect the vibration frequency for further increment.

For 2.5 mm radius fiber sensor, the power loss is too large causing too much attenuation in the signals. Thus, if the external perturbation (vibration in this case) applied to the fiber too intense might cause the power intensity of the propagating light in the fiber sensor all loss into the air and cannot coupling back from the leaky mode to the core mode.

Consequently, the detection range for the sensor at 2.5 mm bend radius is only from 20 Hz to 400 Hz. Thus, bend radius with 5.0 mm is chosen as the optimum bend radius for vibration sensing. Nevertheless, the fiber sensor with bend radius 5.0 mm will still be used in the following field test to test the applicability in real application and provide further evidence that it is the optimum bend radii for the bend coated fiber sensor as compared to others bend radius.

4.3 Field Test (Water Pipeline)

In this section, the bend coated fiber sensor is placed to the water pipeline to test its applicability of vibration sensing in field. The fiber sensor is placed in contact with the pipe wall near to the leak hole as demonstrate in Figure 3.10 in Chapter 3. However, in this field test the frequency of vibration induced by leaking is fluctuating depending the leak size, water pressure, pipe size and type (Hunaidi, 2000).

Hence, the recognition of the signals on background, leak and no leaks can be done by comparing the patterns of the transmitted acoustic waveform and the amplitude of power loss. The background profile in the field test will be used as the

benchmark to indicate the presence of water flow and the occurrence of leakage for the pipeline.

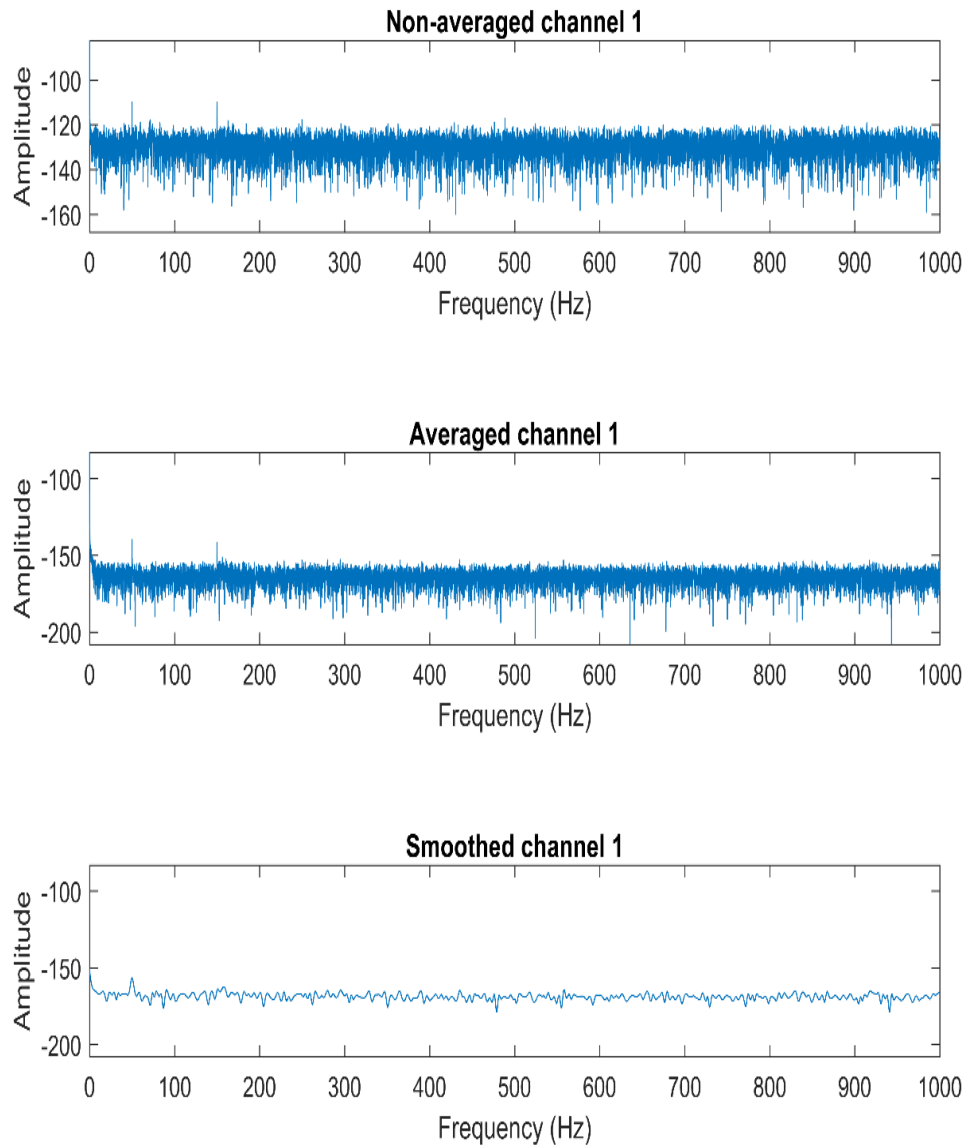
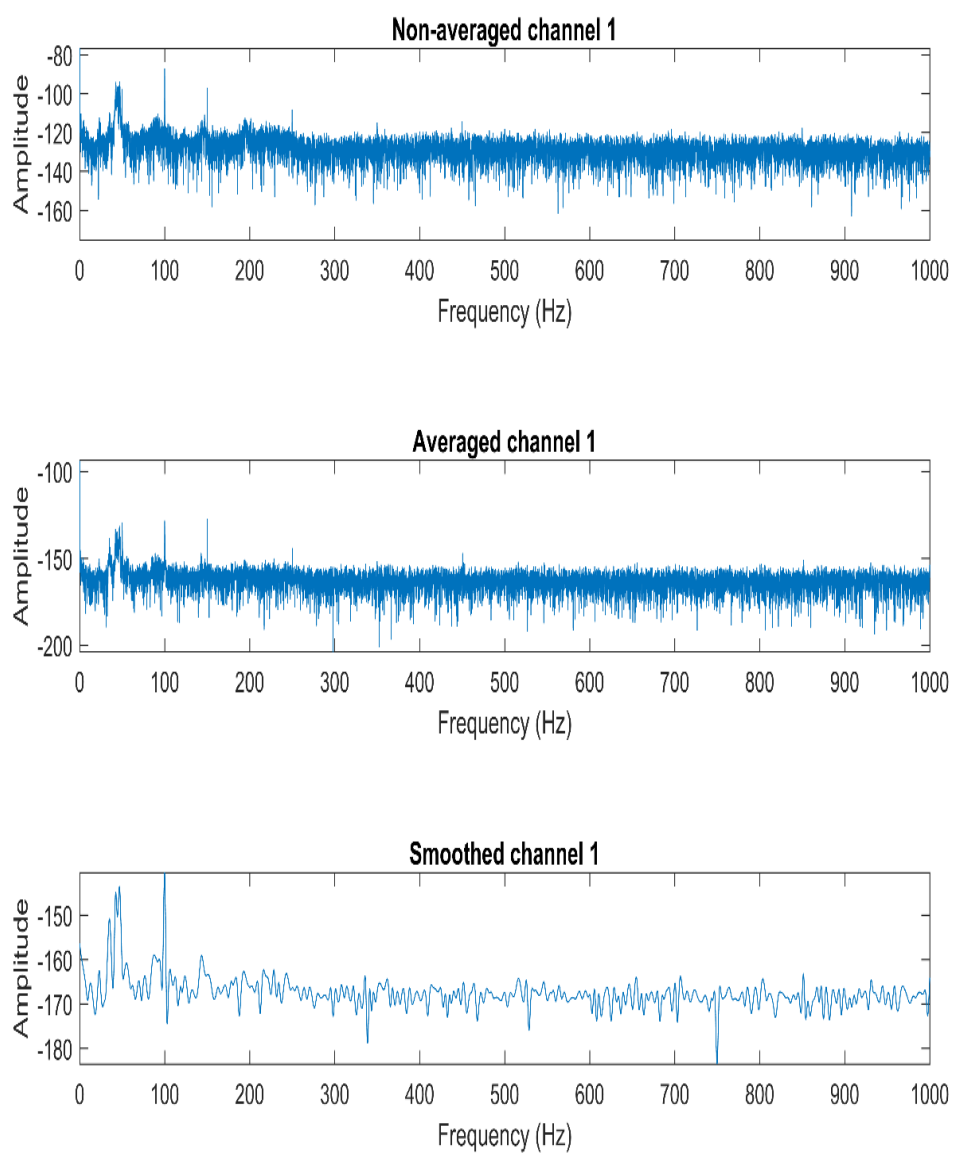


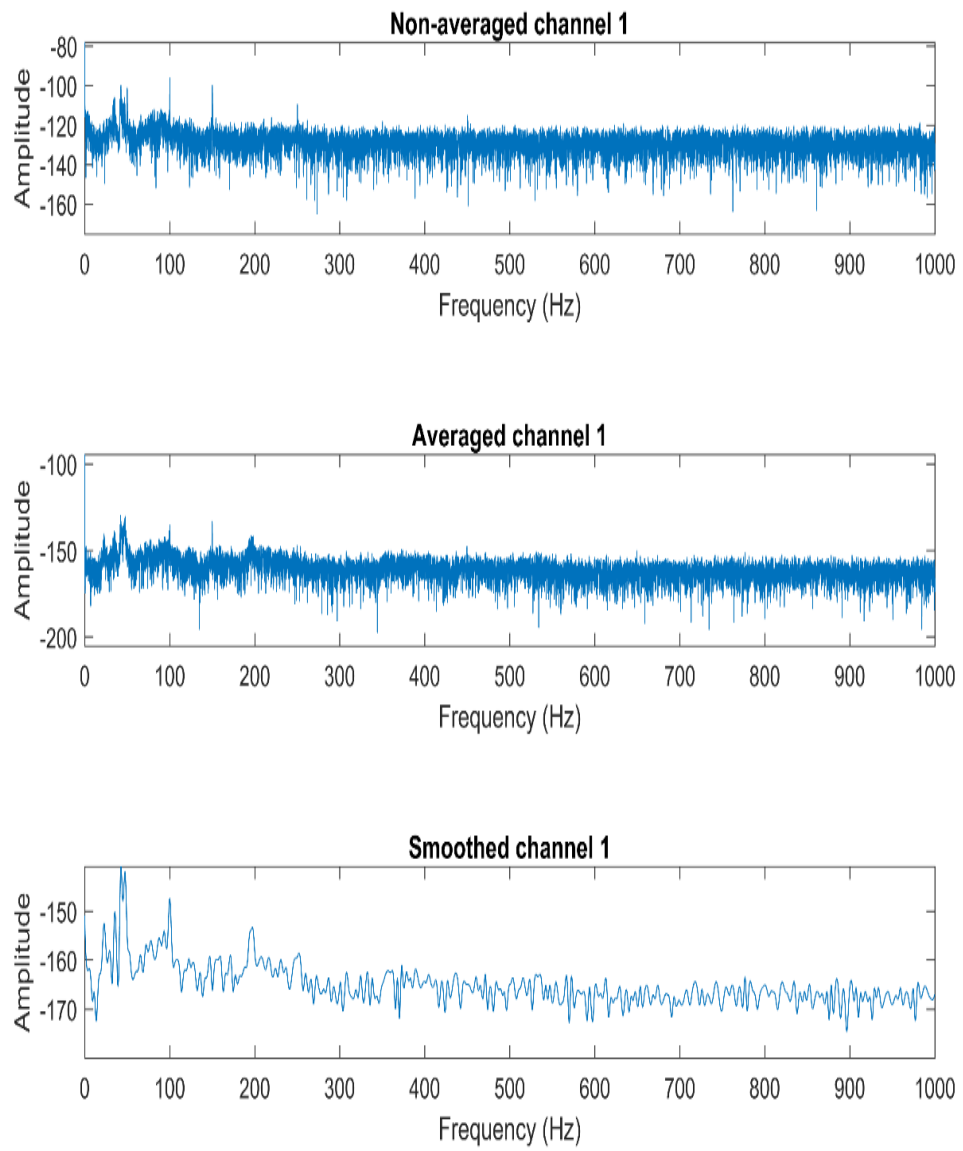
Figure 4.9: Background signals for field test

For 2.5 mm radius, 50 samples of data are collected on no leak (with water flow) and leak conditions. As when the water is pumped into the pipe, a sharp spike shows at 100 Hz with SNR equal to -96.42 dB owing to surge induced vibration

where the velocity of fluid changes causing pressure variation (Wachel and Tison, 1993). Prior to that, the background signal does not have any peaks displayed in the frequency domain as shown in Figure 4.9. Both no leak and leak signals for the 2.5 mm fiber sensor are shown in Figure 4.10 (a) & (b). Obviously, the pattern of the acoustic waves fluctuates from 0 Hz to 250 Hz during the incident of leakage and the SNR different for leak signals are approximated to 25.2 dB.

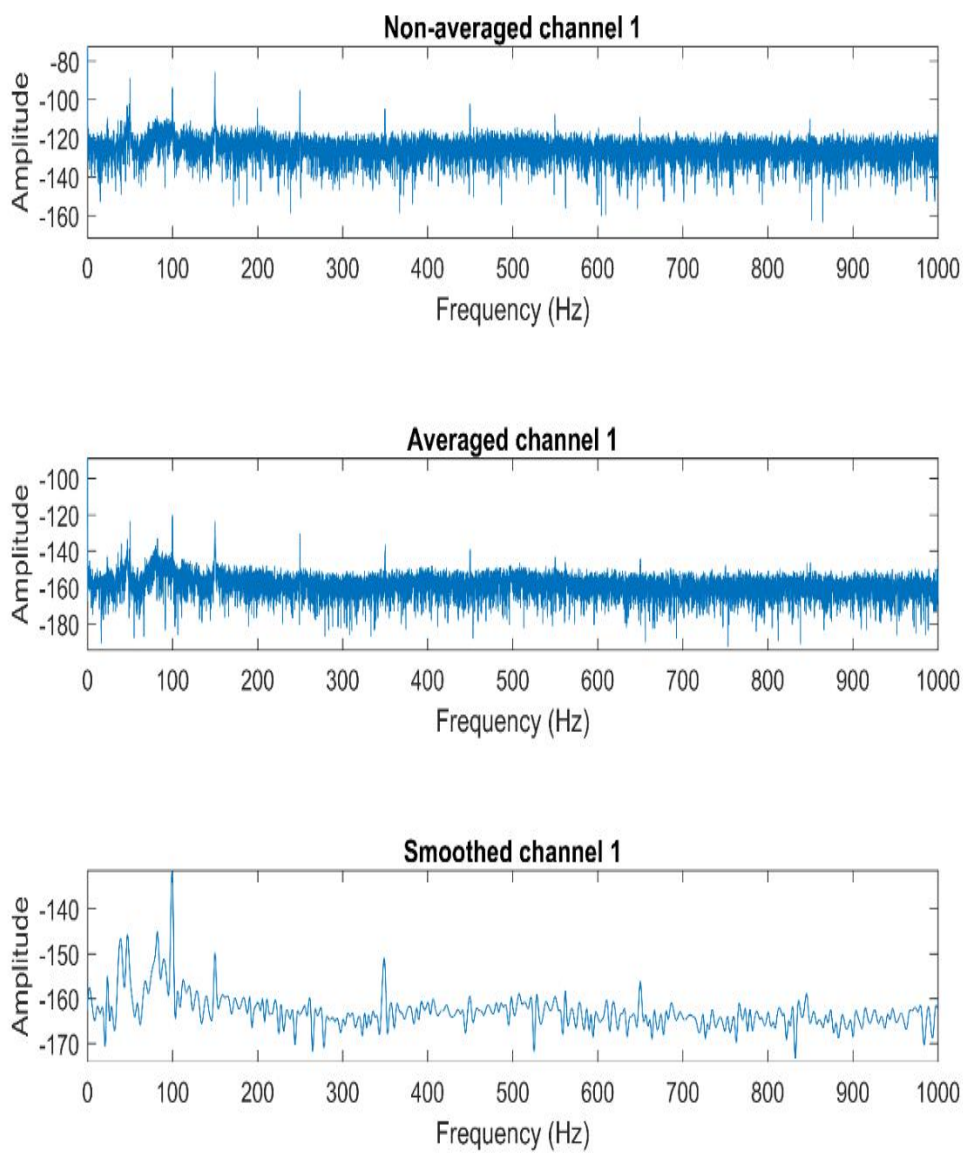


(a)

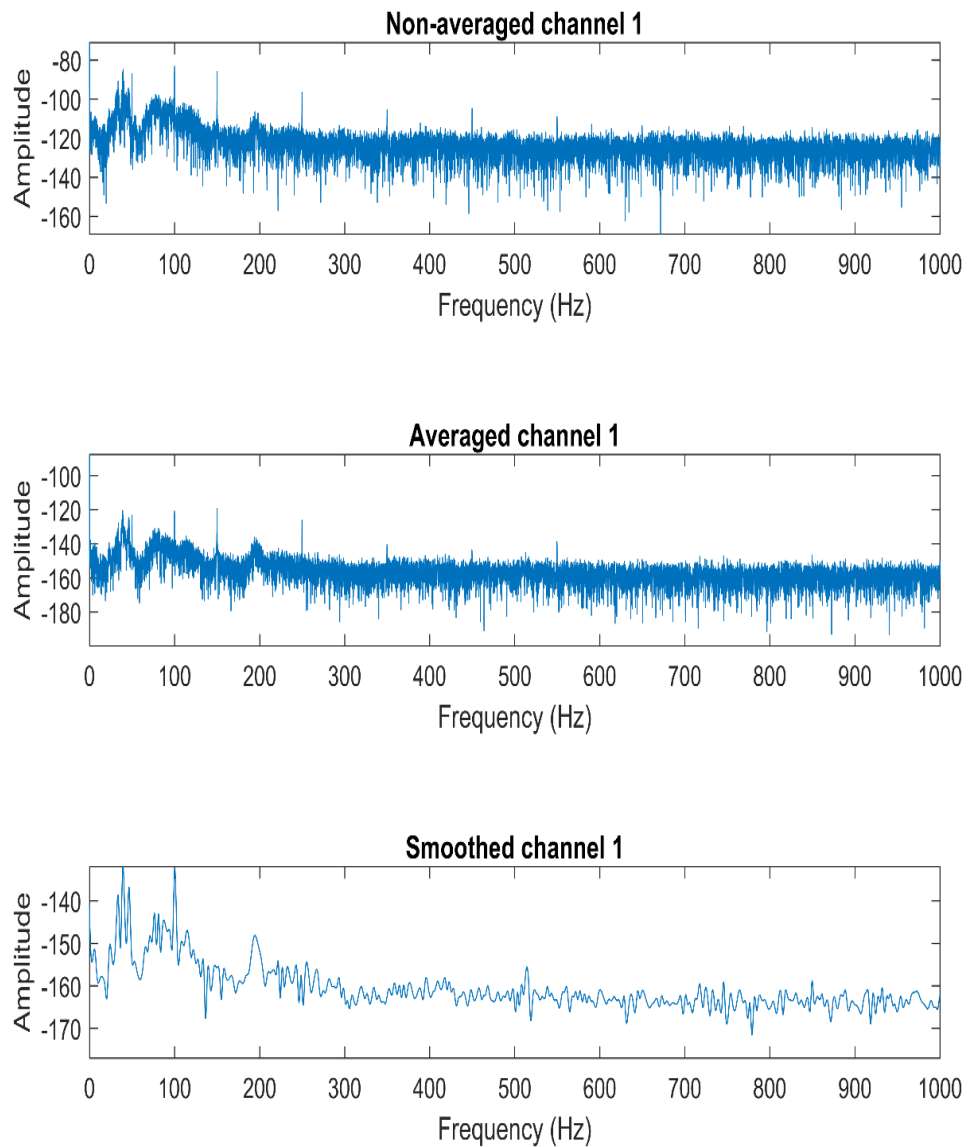


(b)

Figure 4.10: (a) No leak & (b) leak signals for 2.5 mm radius fiber sensor



(a)

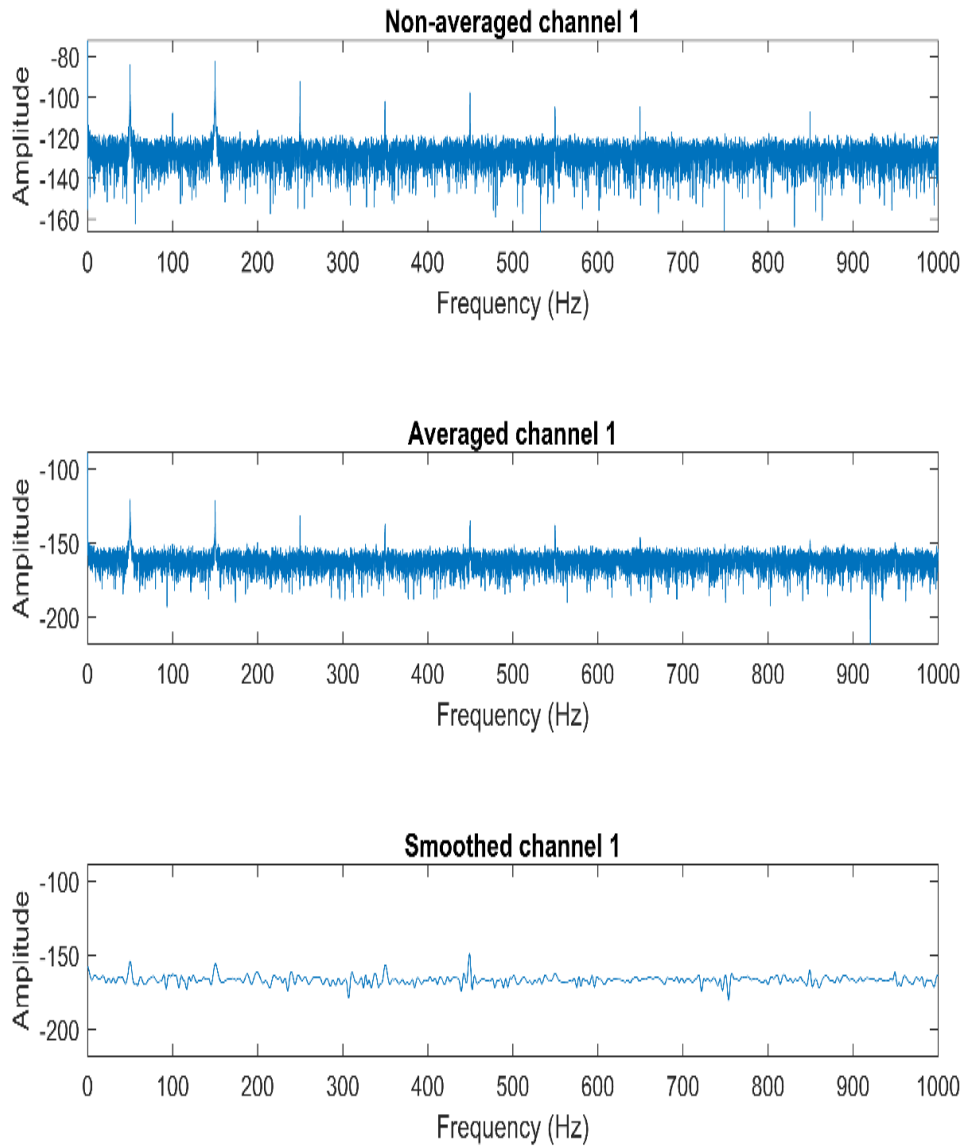


(b)

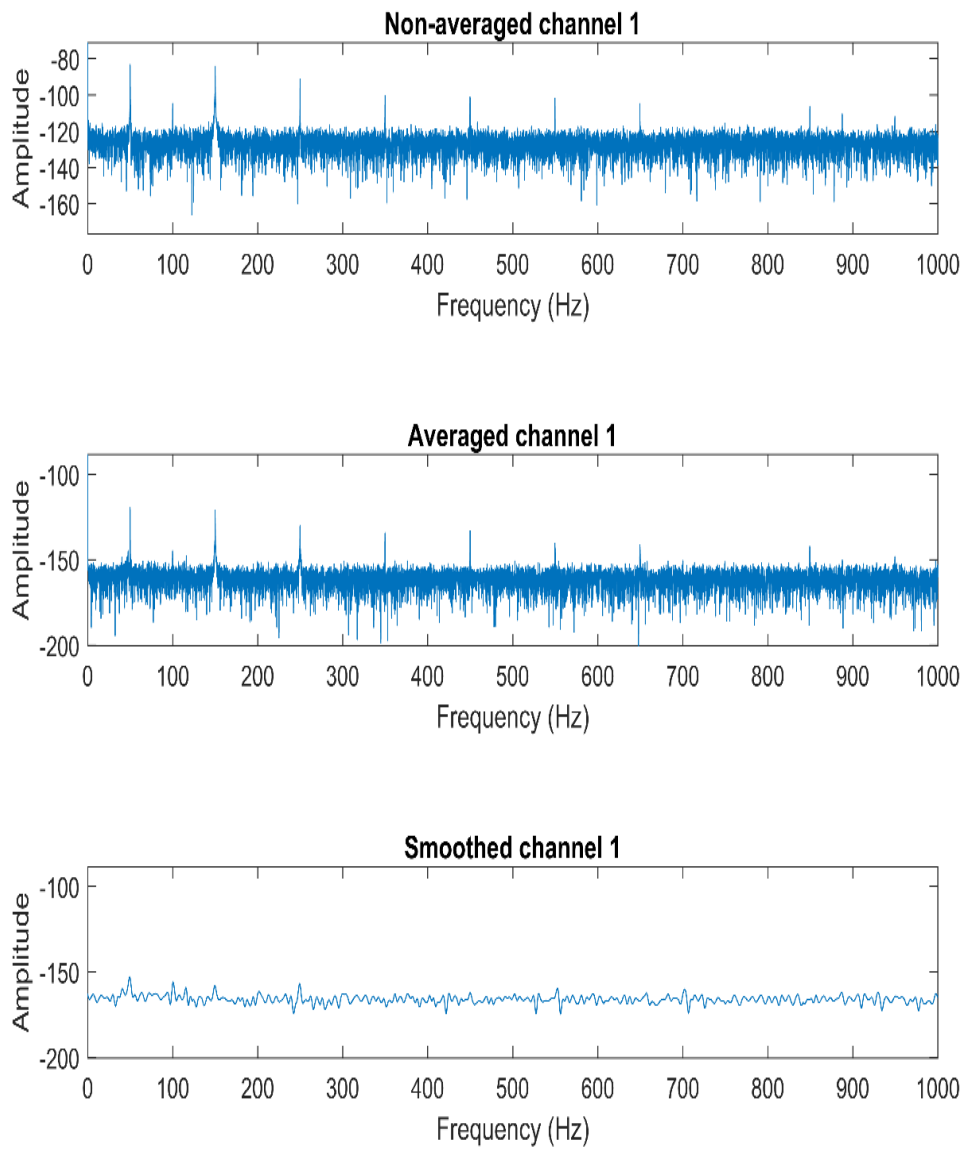
Figure 4.11: (a) No leak & (b) leak signals for 5.0 mm radius fiber sensor

For the 5.0 mm radius, the fiber sensor reveals the same characteristics as in 2.5 mm fiber sensor with a peak frequency at 100 Hz caused by surged vibration when water is pumped into the pipe. At the instance of leakage, the leak signal fluctuates significantly from 0 Hz to 250 Hz causing an overriding region of peaks as illustrated in Figure 4.11 (b). Difference of pressure at the leak hole induced strong

vibration gives significant impact to the 5 mm radius fiber sensor. Besides, SNR of the leak signals for this fiber sensor is approximately 36.8 dB higher than previous 2.5 mm radius fiber sensor which is 25.2 dB.



(a)



(b)

Figure 4.12: (a) No leak & (b) leak signals for 7.5 mm radius fiber sensor

For the 7.5 mm radius, before the no leak and leak signals are processed and filtered there is a peak frequency caused by surged vibration at 100 Hz with SNR equals to -107.8 dB and -104.7 dB respectively depicted in Figure 4.12 (a) & (b). However, owing to the SNR is too low the peak frequency is suppressed together with the unwanted electrical interference after filtering. Furthermore, the signals

from 0 Hz to 250 Hz do not show any fluctuations as compare to previous results during the occurrence of leakage. Consequently, at this bending radius the detection of vibration induced by leakage is not applicable in the field test due to the leak signals having almost the same results as the background signals.

4.4 Summary

In summary, throughout the experiments the bend coated fiber is characterized in different aspects such as bend loss measurements, acoustic vibration test and field test. In the bend loss measurements, the impacts to the fiber sensor is investigated in term of bend radius and wrapping turns of the fiber. The threshold bend radius is found to be 8 mm with bending loss of -2.82 dB.

For the acoustic vibration test, the range of detection of the fiber sensor is determined by the detection of low vibration frequency. And the optimum bending radius for this test is found to be 5 mm with widest sensing range from 20 Hz to 2500 Hz. Last but not least, the applicability of the fiber sensor in the field test is studied carefully by comparing the pattern of the transmitted acoustic waves and the amplitude of power as shown in Figure 4.13. The optimum radius of the fiber sensor in leakage detection is 5 mm with significant overriding region from 0 Hz to 250 Hz and SNR approximate to 36.8 dB.

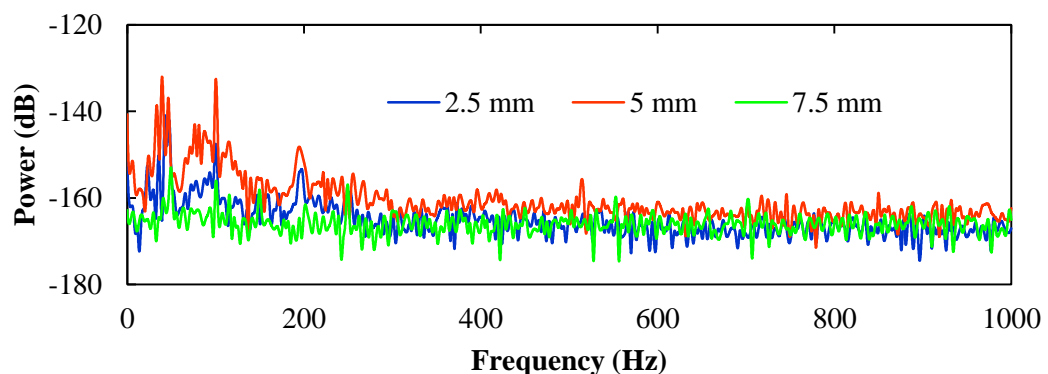


Figure 4.13: Leak signals of the fiber sensor at radius of 2.5, 5.0 and 7.5 mm

CHAPTER 5

CONCLUSIONS AND RECOMMENDATIONS

5.1 Conclusions

Leakage detection is the paramount concern for pipeline security in industry field. However, many systems are inaccessible or isolated, thereupon, in such situation a non-invasive technique is essential.

In this research, a non-intrusive testing technique for the pipeline leakage detection based on the acoustic vibration detection by employing fiber optic sensor was introduced. In the incident of leakage, pipeline system will create the transmission of energy waves e.g. vibrations which are transmitted along the pipe walls. The transmitted energies contain acoustic waves. These measured or logged acoustic waves contain valuable information that can reflect any corrosion or leak occurs in pipelines. Thereupon, through the implementation of the bend coated fiber sensor the acoustic waves will be able detected and condition of the pipe can be determined through analysing of the waveforms.

In conclusion, an acoustic vibration sensor based on macro-bending SMF-28 with simple configuration has been designed and developed. The operation principle of the proposed sensor which utilized the bending loss of bend fiber induced by acoustic vibration. As a result, a simple yet efficient sensor is developed by bending the fiber forming a loop with radius of 5.0 mm and the range of detection for vibration frequency is from 20 Hz to 2500 Hz. No sophisticated feedback or additional accessorial devices are required for the sensing system in the detection of leakage or deformations for pipeline. Moreover, the experimental shows satisfying results for the implementation of localized bend coated fiber sensor in field test. Further work can be extended to determine the location of leakage using distributed sensing through statistical algorithm such as cross-correlation or standard deviation (Hafezi and Mirhosseini, 2015).

5.2 Recommendations for Future Work

In this project the bend coated fiber sensor has been demonstrated and proved its applicability in pipeline leakage detection. However, in order for the fiber sensor to

work in real practice more works are required to be carried on in term of hardware and software.

For the hardware, wavelength dependence property of bending loss in SMF should be taken into account as the wavelength is equally applicable to bend loss as a function of bend radius. Furthermore, the measurement as a function of wavelength is prospectively to be more accurate due to no mechanical adjustment is needed in the experiment (Morgan, Barton, Harper and Jones, 1990).

In addition, more factors should be taken into considerations in real application such as the sizes or shapes of leakage, position of pipeline (buried in wall or under the soil) and so on. Therefore, in the software part, an automated signal processing system is required in filtering the unwanted noise and improve signal to noise ratio (SNR) of the collected data. Eventually, this would greatly enhance the data processing time and ameliorate the signal interpretation.

REFERENCES

- Badar, A. and Maclean, T., 1991. Transition and pure bending losses in multimode and single-mode bent optical fibres. *IEE Proceedings J-Optoelectronics*, 138(4), pp.261–268.
- Chung, D., 2001. Structural health monitoring by electrical resistance measurement. *Smart materials and structures*, 10(4), p.624.
- Fidanboyly, K. and Efendioglu, H., 2009. Fiber optic sensors and their applications. In: *5th International Advanced Technologies Symposium (IATS'09)*.
- Gambling, W. and Matsumura, H., 1978. Propagation characteristics of curved optical fibers. *IEICE TRANSACTIONS (1976-1990)*, 61(3), pp.196–201.
- Gambling, W., Matsumura, H., Ragdale, C. and Sammut, R., 1978. Measurement of radiation loss in curved single-mode fibres. *IEE Journal on Microwaves, Optics and Acoustics*, 2(4), pp.134–140.
- Hafezi, M.M. and Mirhosseini, M., 2015. Application of Cross-Correlation in Pipe Condition Assessment and Leak Detection; Using Transient Pressure and Acoustic Waves. *Resources and Environment*, 5(5), pp.159–166.
- Harris, A. and Castle, P., 1986. Bend loss measurements on high numerical aperture single-mode fibers as a function of wavelength and bend radius. *Journal of Lightwave technology*, 4(1), pp.34–40.
- Hu, R.P. and Huang, X.G., 2009. A simple fiber-optic flowmeter based on bending loss. *IEEE Sensors journal*, 9(12), pp.1952–1955.
- Huang, Y., Guo, T., Lu, C. and Tam, H.-Y., 2010. VCSEL-based tilted fiber grating vibration sensing system. *IEEE Photonics Technology Letters*, 22(16), pp.1235–1237.
- Hunaidi, O., 2000. Detecting leaks in water-distribution pipes. *Construction Technology Update*, 40, pp.1–6.
- Kasap, S.O., 2001. *Optoelectronics and Photonics: Principles and Practices*. Prentice-Hall, New Jersey.
- Kepak, S., Cubik, J., Doricak, J., Vasinek, V., Siska, P., Liner, A. and Papes, M., 2013. The arms arrangement influence on the sensitivity of Mach-Zehnder fiber optic interferometer. In: *SPIE Optics+ Optoelectronics*. pp.877415–1–877415–8.
- Lee, B., 2003. Review of the present status of optical fiber sensors. *Optical fiber technology*, 9(2), pp.57–79.

- Morgan, R., Barton, J.S., Harper, P.G. and Jones, J.D., 1990. Wavelength dependence of bending loss in monomode optical fibers: effect of the fiber buffer coating. *Optics letters*, 15(17), pp.947–9.
- Murakami, Y. and Tsuchiya, H., 1978. Bending losses of coated single-mode optical fibers. *IEEE Journal of Quantum Electronics*, 14(7), pp.495–501.
- Neumann, E.G., 2013. *Single-mode fibers: fundamentals*. Springer.
- Nishino, Z.T., Chen, K. and Gupta, N., 2014. Power modulation-based optical sensor for high-sensitivity vibration measurements. *IEEE Sensors Journal*, 14(7), pp.2153–2158.
- PHMSA, U., 2011. Data & Statistics: Distribution, Transmission, and Liquid Annual Data. *US Department of Transportation, Pipeline and Hazardous Materials Safety Administration*.
- Polygerinos, P., Seneviratne, L.D. and Althoefer, K., 2011. Modeling of light intensity-modulated fiber-optic displacement sensors. *IEEE Transactions on Instrumentation and Measurement*, 60(4), pp.1408–1415.
- Rajan, G., 2015. *Optical fiber sensors: advanced techniques and applications*. CRC press.
- Reed, C., Robinson, A.J. and Smart, D., 2004. *Techniques for monitoring structural behaviour of pipeline systems*. American Water Works Association.
- Righini, G.C., Tajani, A. and Cutolo, A., 2009. *An introduction to optoelectronic sensors*. World Scientific.
- Shahami, bin S., Siti Azlida, binti I. and Dambul, K.D., 2016. Sensitivity improvement in a fiber macrobending refractive index sensor. In: *Photonics (ICP), 2016 IEEE 6th International Conference on*. pp.1–3.
- Snyder, A.W. and Love, J.D., 1986. Optical waveguide theory. *J. Opt. Soc. Am. A*, 3, p.378.
- Steele, W.H., 1983. *Interferometry*. CUP Archive.
- Tsao, S.L. and Cheng, W.M., 2002. Simplified formula of bending loss for optical fiber sensors. *Fiber & Integrated Optics*, 21(5), pp.333–344.
- Tubb, R., 2017. Pipeline & Gas Journal's 2017 Worldwide Pipeline Construction Report. *Pipeline & Gas Journal*.
- Wachel, J. and Tison, J., 1993. *Vibrations in reciprocating machinery and piping systems*. Engineering Dynamics Incorporated.

- Wang, P., Semenova, Y., Sun, A., Wu, Q. and Farrell, G., 2010. A macrobending fiber based vibration sensor using Whispering Gallery mode. In: *Proc. of SPIE Vol.* pp.772623–1.
- Wang, X.J., Lambert, M.F., Simpson, A.R. and Vitkovsky, J.P., 2001. Leak detection in pipelines and pipe networks: a review. In: *6th Conference on Hydraulics in Civil Engineering: The State of Hydraulics; Proceedings.* p.391.
- Wild, G. and Hinckley, S., 2007. Fiber Bragg grating sensors for acoustic emission and transmission detection applied to robotic NDE in structural health monitoring. In: *Sensors Applications Symposium, 2007. SAS'07. IEEE.* pp.1–6.
- Wolinski, T., 1999. Polarization in optical fibers. *Acta Physica Polonica A*, 95(5), pp.749–760.
- Xu, B., Li, Y., Sun, M., Zhang, Z.W., Dong, X.Y., Zhang, Z.X. and Jin, S.Z., 2012. Acoustic vibration sensor based on nonadiabatic tapered fibers. *Optics letters*, 37(22), pp.4768–4770.
- Xu, S., Liang, Y., Xu, G. and Qu, D., 2011. An experimental research of fiber acoustic emission detection based on multimode fiber. In: *Optoelectronics and Microelectronics Technology (AISOMT), 2011 Academic International Symposium on.* pp.60–64.
- Yang, L., Liu, G., Zhang, G. and Gao, S., 2009. Sensor development and application on the oil-gas pipeline magnetic flux leakage detection. In: *Electronic Measurement & Instruments, 2009. ICEMI'09. 9th International Conference on.* pp.2–876.
- Yang, Y., Hu, Y. and Lu, Y., 2008. Sensitivity of PZT impedance sensors for damage detection of concrete structures. *Sensors*, 8(1), pp.327–346.
- Yin, S. and Yu, F., 2002. *Fiber optic sensors.* Wiley Online Library.
- Zhang, Y. and Ball, G., 2001. Fiber mini-bend light guide.
- Zhao, Y., Jin, Y. and Liang, H., 2011. Investigation on single-mode-multimode-single-mode fiber structure. In: *Photonics and Optoelectronics (SOPO), 2011 Symposium on.* pp.1–4.

APPENDICES

APPENDIX A: CALCULATION OF MINIMUM CRITICAL BEND RADIUS FOR SINGLE MODE FIBER

Based on the Corning SMF-28 datasheet, the refractive index difference, Δ and refractive index for core, n_1 are 0.0036 and 1.4682 respectively. Thus, the refractive index for clad, n_2 can be calculated as

$$\Delta = \frac{n_1 - n_2}{n_1}$$

$$n_2 = (1.4682) - (0.0036)(1.4682) = 1.4629$$

The core radius, a and cut-off V -number are 4.15 μm and 2.405 respectively. The cut-off frequency, λ_c is given as below

$$\lambda_c = \frac{2\pi a}{V} \left(\sqrt{n_1^2 - n_2^2} \right) = 1351 \text{ nm}$$

The numerical aperture, NA is calculated as below

$$NA = (n_1^2 - n_2^2)^{\frac{1}{2}} = 0.13$$

The relative difference of refractive index, Δ_n is given by

$$\Delta_n \approx \frac{NA^2}{2n_1} \approx 5.8 \times 10^{-3}$$

Finally, the minimum critical bend radius, R_c is obtained

$$R_c \approx \frac{20\lambda}{\sqrt[3]{\Delta_n}} \left[2.748 - 0.996 \left(\frac{\lambda}{\lambda_c} \right) \right]^{-3} \approx 16 \text{ mm}$$

APPENDIX B: CORNING SMF-28 DATA SHEET

Optical Specifications**Attenuation**

Wavelength (nm)	Attenuation* (dB/km)		
	Premium		Standard
1310	≤ 0.34	≤	0.35
1550	≤ 0.20	≤	0.22

*Alternate attenuation values available upon request

Point Discontinuity

No point discontinuity greater than 0.10 dB at either 1310 nm or 1550 nm.

Attenuation at the Water Peak

The attenuation at 1383 ± 3 nm shall not exceed 2.1 dB/km.

Attenuation vs. Wavelength

Range (nm)	Ref. λ (nm)	Max. α Difference (dB/km)
1285 - 1330	1310	0.05
1525 - 1575	1550	0.05

*The attenuation in a given wavelength range does not exceed the attenuation of the reference wavelength (λ) by more than the value α

Attenuation with Bending

Mandrel Diameter (mm)	Number of Turns	Wavelength (nm)	Induced Attenuation* (dB)
32	1	1550	≤ 0.50
50	100	1310	≤ 0.05
50	100	1550	≤ 0.10
60	100	1550	≤ 0.05

*The induced attenuation due to fiber wrapped around a mandrel of a specified diameter.

Cable Cutoff Wavelength (λ_{ccf})

$$\lambda_{ccf} \leq 1260 \text{ nm}$$

Mode-Field Diameter

$$9.2 \pm 0.4 \text{ } \mu\text{m at 1310 nm}$$

$$10.4 \pm 0.8 \text{ } \mu\text{m at 1550 nm}$$

Environmental Specifications

Environmental Test Condition	Induced Attenuation 1310 nm/1550 nm (dB/km)	
Temperature Dependence -60° C to +85° C *	δ	0.05
Temperature- Humidity Cycling -10° C to +85° C*,	δ	0.05

up to 98% RH		
Water Immersion, 23°± 2° C*	δ	0.05
Heat Aging, 85° ± 2° C*	δ	0.05

*Reference temperature = +23° C

Operating Temperature Range

-60 °C to +85 °C

Dimensional Specifications

Length (km/reel): fiber lengths available up to 50.4*

* Longer spliced lengths available at a premium.

Glass Geometry

Fiber Curl: ε 4.0 m radius of curvature

Cladding Diameter: 125.0 ± 0.7 μm

Core-Clad Concentricity: δ 0.5 μm

Cladding Non-Circularity: δ 1.0%

Coating Geometry

Coating Diameter: 245 ± 5 μm

Coating-Cladding Concentricity: <12 μm

Performance Characterizations

Core Diameter: 8.2 μm

Numerical Aperture: 0.14

*NA is measured at the one percent power level of a one-dimensional far-field scan at 1310 nm.

Zero Dispersion Wavelength (λ₀): 1313 nm

Zero Dispersion Slope (S₀): 0.086 ps / (nm²·km)

Refractive Index Difference: 0.36%

Effective Group Index of Refraction,

(N_{eff} @ nominal MFD):

1.4677 at 1310 nm

1.4682 at 1550 nm

Fatigue Resistance Parameter (n_d): 20

Coating Strip Force:

Dry: 0.6 lbs. (3N)

Wet, 14-day room temperature: 0.6 lbs. (3N)

Rayleigh Backscatter Coefficient (for 1 ns pulse width):

1310 nm: -77 dB

1550 nm: -82 dB